The Canadian Mineralogist
Vol. 45, pp. 723-750 (2007)
DOI: 10.2113/gscanmin.45.4.723

THE GENESIS OF SULFIDE ASSEMBLAGES IN THE FORMER WILHELMINE MINE, SPESSART, BAVARIA, GERMANY

MARTIN OKRUSCH[§]

Mineralogisches Institut, Universität Würzburg, Am Hubland, D–97074 Würzburg, Germany

JOACHIM A. LORENZ

Graslitzer Str. 5, D–63791 Karlstein am Main, Germany

STEFAN WEYER

Institut für Petrologie, Geochemie und Lagerstättenkunde, Universität Frankfurt am Main, Senckenberganlage 28, D–60325 Frankfurt am Main, Germany

ABSTRACT

The vein-type copper mineralization in the abandoned Wilhelmine copper mine, Sommerkahl, Spessart, northwestern Bavaria, Germany, is hosted by metamorphic rocks of the Spessart Crystalline Complex. These are overlain by Permo-Triassic sedimentary rocks, including the stratabound base-metal mineralization of the Kupferschiefer. Ore textures in the sulfide veins demonstrate three stages of mineralization: (i) An early stage (I) is characterized by colloform textures, documented by spherical, cockade-like or garland-shaped, monomineralic or polymineralic aggregates of tennantite I, enargite I, pyrite I, chalcopyrite I, bornite I and digenite I. (ii) During a subsequent stage of recrystallization (II), the colloform textures were overgrown by, or enclosed in, anhedral grains of tennantite II, enargite II, bornite II, digenite II, pyrite II and chalcopyrite II. Minimum temperatures of about 175°C for this stage can be estimated from the bulk composition of fine-grained to submicroscopic digenite–bornite intergrowths, exsolved from an initial 1*a* solid solution with up to 55 mole % of bornite. Conversely, the assemblage pyrite + chalcopyrite + tennantite provides an uppermost temperature limit of ~440°C [at an $a(S_2) = 10^{-5}$]. (iii) A late stage of alteration (III) led to the replacement of the primary sulfides by yarrowite, spionkopite and rare covellite, together with goethite, under decreasing temperatures and rising activity of sulfur. The close spatial association of the Sommerkahl vein-type Cu deposit with the overlying Kupferschiefer suggests that this metal-rich bituminous shale played an important role in the formation of the ore veins. Sulfur isotope analyses yielded negative $\delta^{34}S$ of –12.8 to –23.9‰, which indicate that the sulfur was derived from the overlying Kupferschiefer, presumably by hydrothermal leaching. Such a low-temperature mobilization could also be discussed for all or part of the metals forming the Wilhelmine ore, which later on recrystallized in response to hydrothermal activity (modified hydrothermal model). However, we prefer a strictly hydrothermal model, according to which all or most of the metals were derived from deep-seated sources, transported upward by hydrothermal fluids, and precipitated by thermochemical reduction of sulfate due to interaction with the sulfur-bearing organic matter and the pyrite of the Kupferschiefer. Formation of the sulfide ore veins in the former Wilhelmine mine is related to post-Variscan hydrothermal activity that affected the Spessart area in Middle Jurassic to late Early Cretaceous time.

Keywords: vein-type Cu mineralization, Kupferschiefer, tennantite, bornite, digenite, anilite, yarrowite, spionkopite, sulfur isotopes, hydrothermal activity, thermochemical sulfate reduction, Spessart, Germany.

SOMMAIRE

La minéralisation cuprifère en veines à la mine abandonnée de Wilhelmine, à Sommerkahl, Spessart, au nord-ouest de la Bavière, en Allemagne, est encaissée dans les roches métamorphiques du complexe cristallin de Spessart. Ces roches sont recouvertes de roches sédimentaires permo-triassiques, dont la séquence stratifiée minéralisée en métaux de base de Kupferschiefer. Les textures du minerai dans ces veines montrent trois stades de minéralisation: (i) un stade précoce (I) a donné des textures colloformes, et des aggrégats sphériques, en cockade ou en guirlandes, soit monominérales ou polyminérales, de tennantite I, énargite I, pyrite I, chalcopyrite I, bornite I et digénite I. (ii) Au cours du stade of recristallisation (II) qui a suivi, les textures colloformes ont été recouvertes par ou incluses dans des grains xénomorphes de tennantite II, énargite II, bornite II, digénite II, pyrite II et chalcopyrite II. Une température minimale d'environ 175°C au stade II découle de la composition globale d'intercroissances à

§ *E-mail address*: okrusch@mail.uni-wuerzburg.de

granulométrie fine, voire submicroscopiques, de digénite avec bornite, produits de l'exsolution d'une solution solide originale 1*a* ayant plus de 55% (base molaire) de bornite. Par contre, l'assemblage pyrite + chalcopyrite + tennantite indique une température maximale d'environ ~440°C [à une valeur de $a(S_2)$ égale à 10^{-5}]. (iii) Un stade tardif d'altération (III) a causé le remplacement des sulfures primaires par yarrowite, spionkopite et covellite plus rare, avec la goethite, dans un régime de baisse de températures et d'augmentation de l'activité du soufre. L'étroite association dans l'espace du gisement cuprifère en veines de Sommerkahl avec les horizons argileux minéralisés du Kupferschiefer peut faire penser que cet horizon bitumineux enrichi en métaux a exercé un rôle important dans la formation des veines. Les analyses des isotopes de soufre ont donné des valeurs négatives de $\delta^{34}S$, entre –12.8 et –23.9‰, indication que le soufre est dérivé de la séquence Kupferschiefer par lessivage hydrothermal. Une telle mobilisation à faible température pourrait s'appliquer à toutes les composantes du minerai à la mine Wilhelmine, qui par la suite aurait subi une recristallisation en réponse à une activité hydrothermale (selon le modèle hydrothermal modifié). Toutefois, nous préférons un modèle hydrothermal plus pur, selon lequel tous les métaux, ou la plupart, sont dérivés d'une source profonde, transportés par des fluides hydrothermaux ascendants, et précipités par réduction thermochimique de sulfates suite à une interaction avec la matière organique porteuse de soufre et la pyrite du Kupferschiefer. La formation des veines de sulfures à la mine Wilhelmine est liée au créneau d'activité hydrothermale post-Varisque qui a affecté la région de Spessart du Jurassique moyen jusqu'à la fin du Crétacé précoce.

(Traduit par la Rédaction)

Mots-clés: minéralisation cuprifère en veines, Kupferschiefer, tennantite, bornite, digénite, anilite, yarrowite, spionkopite, isotopes de soufre, activité hydrothermale, réduction thermochimique de sulfate, Spessart, Allemagne.

Introduction

In central Europe, the incidence of tectonically controlled vein-type mineralization of base and precious metals, barite and barite–fluorite is closely related to the post-Variscan unconformity (*e.g.*, Dill 1988, Shepherd *et al.* 2005). Some of the deposits, especially those with base metals, occur just below or within the stratabound Cu–Zn–Pb–Ag deposits of the Upper Permian Kupferschiefer (copper shale; *e.g.*, Kulick *et al.* 1984, Schmidt *et al.* 1986, Vaughan *et al.* 1989, Speczik 1995, Blundell *et al.* 2003). Examples are the northwestern Spessart in Hesse and northwestern Bavaria (*e.g.*, Wagner & Lorenz 2002), the Richelsdorf area in Hesse (*e.g.*, Messer 1955,

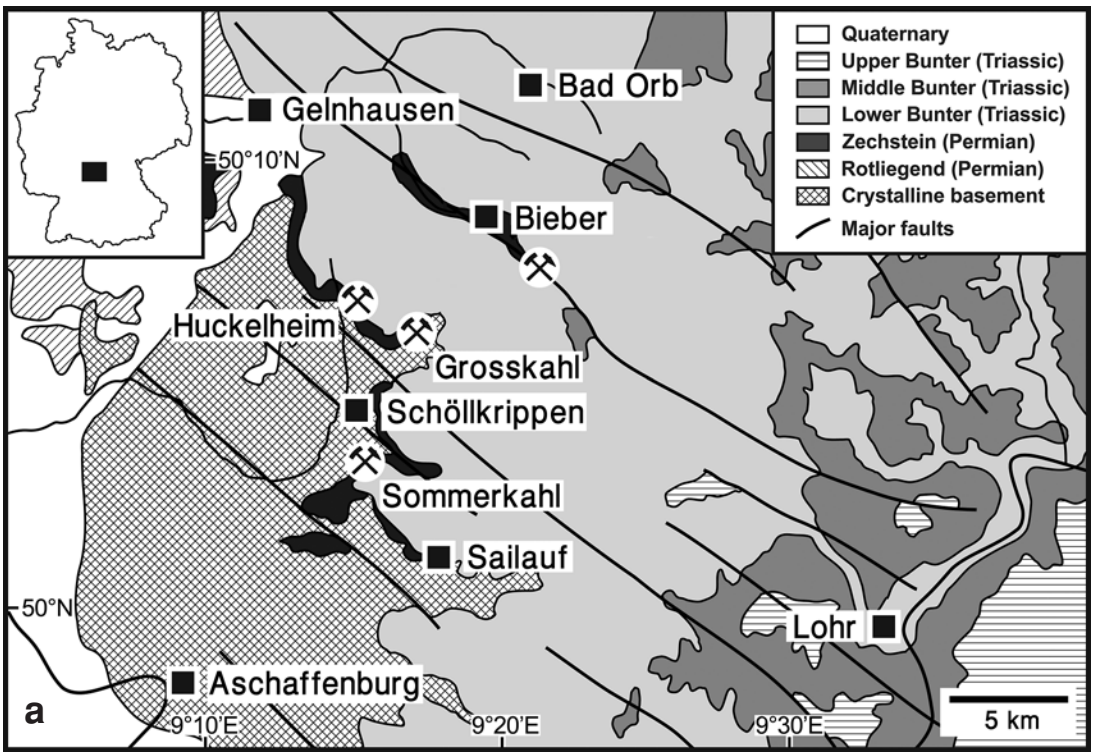

Tobschall *et al*. 1986), and the Mansfeld–Sangerhausen district in Sachsen–Anhalt (*e.g.*, Gerlach 1992). The close spatial association of both types of deposits indicates that a genetic link may exist between them. For example, the metal content of the ore veins may have been derived from the Kupferschiefer by some leaching process or, alternatively, the Kupferschiefer acted merely as a trigger for the precipitation of metal sulfides from hydrothermal solutions.

In northwestern Spessart, several vein-type base-metal deposits are hosted by mica schists, paragneisses and orthogneisses of the crystalline basement, but also extend into the overlying Upper Permian sedimentary strata, including the Kupferschiefer (Figs. 1a, b). Both the vein-style and the stratabound Kupferschiefer base-metal mineralization have been mined intermittently from the 16th to the beginning of the 20th century (Freymann 1991, and references herein). In the abandoned Wilhelmine copper mine at Sommerkahl, cataclastic orthogneiss is cross-cut and impregnated by small veins, which consist of pyrite and copper sulfides. Among these, tennantite and chalcopyrite are ubiquitous, whereas bornite, enargite, digenite – djurleite – anilite and yarrowite – spionkopite – covellite form minor but important constituents in some of the samples investigated. The mine was operated during the 18th century, with renewed mining activities from 1871 to 1892 and from 1916 to 1922 (Freymann 1991).

Prompted by the close spatial association of the vein-type mineralization in the Wilhelmine mine with the overlying Kupferschiefer, a discussion of a hypogene *versus* supergene genesis of the copper mineralization started in the late 19th century. Judging from the fact that the copper ore occurs in veins, which fill fractures and fissures in the gneiss, Bücking (1892) assumed a hydrothermal origin, similar to the cobalt vein-type deposits of the so-called "Kobaltrücken" in the nearby mining districts of Bieber (Fig. 1a). By contrast, Thürach (1893) proposed that the copper ore was derived from the Upper Permian Kupferschiefer, overlying the crystalline basement only about 10 – 50 m above the mine (Figs. 1b, 2). A supergene formation was also favored by von Gehlen (1964), who assumed that the supergene solutions seeped into open fissures of the sea floor at the beginning of the Kupferschiefer sedimentation. In contrast, Okrusch & Weinelt (1965) favored a secondary redeposition of initially hydrothermal ore by supergene solutions.

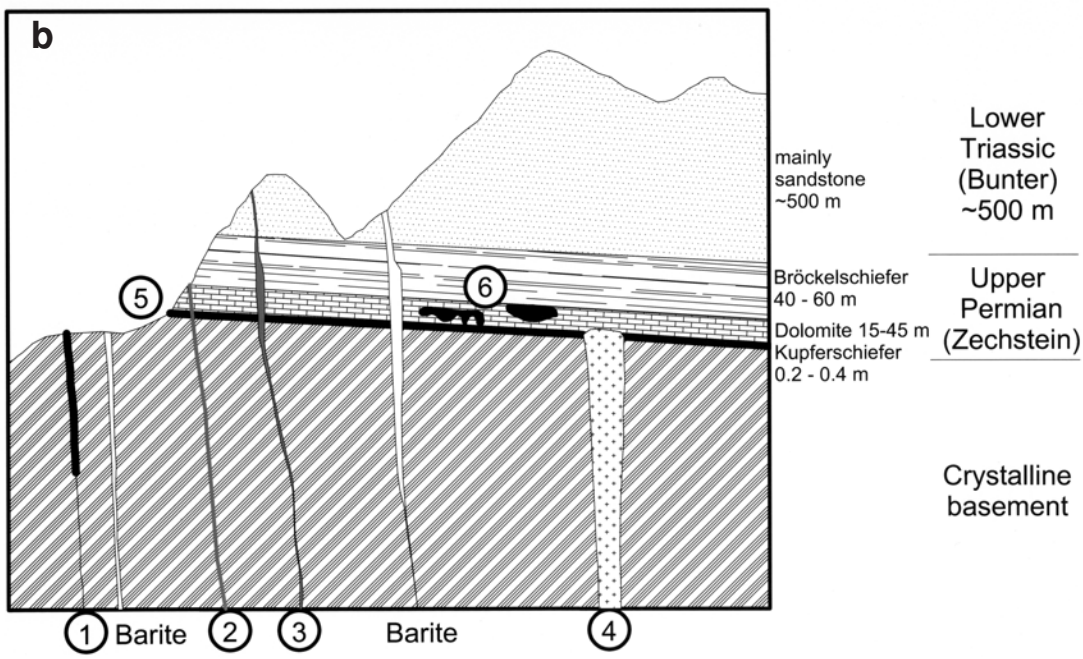

FIG. 1. a) Geological sketch-map of the northwestern Spessart showing the location of vein-style sulfide deposits, after Wagner & Lorenz (2002). The Wilhelmine mine is situated in the village of Sommerkahl. b) Schematic profile (not to scale) showing the main types of post-Variscan mineralization of the Spessart in the crystalline basement and the sedimentary strata of Upper Permian and Lower Triassic age (modified after Freymann 1991). (1) Vein-type Cu–Fe–As mineralization in the Variscan basement at Sommerkahl; (2) vein-type Cu–As–Ag–Pb–Zn mineralization at Huckelheim and Grosskahl; (3) Co–Ni–Bi mineralization at Bieber; (4) hydrothermal Mn–As–Bi mineralization in the Lower Permian rhyolite at Sailauf; (5) Kupferschiefer; (6) Fe–Mn mineralization in dolomites of the Zechstein (Upper Permian).

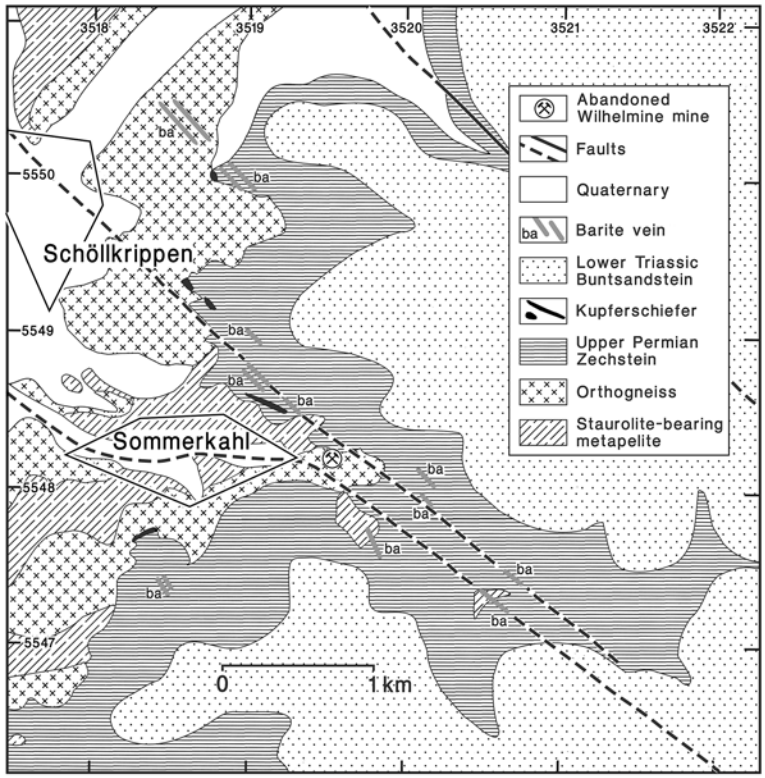

FIG. 2. Geological situation of the Schöllkrippen – Sommerkahl area in the northwestern Spessart. It should be noted that the Kupferschiefer is preserved only as erosional relics in valleys, depressions and narrow passes. The areas taken by the village of Sommerkahl and the town of Schöllkrippen are designated by polygons. The four-digit numbers at the horizontal and vertical margins of the map indicate the coordinates of the German Gauss–Krüger grid (after Okrusch & Weinelt 1965).

In spite of the controversy regarding their genetic interpretation, the assemblages of ore minerals of the Wilhelmine deposit have not been studied in detail. Recent rehabilitation operations in one of the underground galleries, prompted by the establishment of a visitor's mine, produced a wealth of fresh samples of ore, which facilitated detailed studies of the ore textures and comprehensive electron-microprobe analyses of the sulfide minerals.

Earlier results of sulfur isotope analyses, performed on unspecified samples of ore from the Wilhelmine mine, seem to indicate that the sulfur was indeed derived from the overlying Kupferschiefer (Hahn-Weinheimer in Okrusch & Weinelt 1965). In order to test this assumption, sulfur isotope compositions of individual sulfide phases were determined by laser-ablation, multichannel ICP–MS.

Our results place constraints on the ore-forming process in the Wilhelmine mine and may shed some light on the petrogenesis of similar Kupferschiefer-related, vein-type deposits in central Europe.

GEOLOGY

General overview

The Spessart Crystalline Complex, a constituent of the Mid-German Crystalline Rise, consists of a sequence of northeast-trending units of metasedimentary, metagranitic and metabasic lithologies (*e.g.*, Okrusch & Weber 1996, and references herein). During the Variscan Orogeny, the protoliths were deformed and metamorphosed under medium-pressure amphibolite-facies conditions, with a clockwise P–T path that reached about 620°C and 5 to 7 kbar at the metamorphic peak (*e.g.*, Okrusch 1995, Will 1998). K–Ar and Ar–Ar dates on hornblende, muscovite and biotite from various rock-types indicate uplift and cooling of the crystalline

basement in a narrow time-span between 325 and 315 Ma (Lippolt 1986, Nasir *et al.* 1991, Dombrowski *et al.* 1994).

In the central part of the Spessart Crystalline Complex (Figs. 1a, 2), staurolite-bearing metapelites of the Cambro-Ordovician Mömbris Formation are intercalated with orthogneiss of the so-called Rotgneiss Complex (Matthes & Okrusch 1965), which hosts the Wilhelmine mine. Confirming earlier results of Rb–Sr whole-rock dating (Kreuzer *et al.* 1973, Lippolt 1986, Nasir *et al.* 1991), Dombrowski *et al.* (1995) dated the protolith age of the orthogneiss at 418 ± 18 Ma, using the $^{207}Pb/^{206}Pb$ evaporation method on single crystals of zircon. Judging from geochemical evidence, the orthogneiss is intermediate in character between I-type and S-type granites, with a relatively low $^{87}Sr/^{86}Sr$ initial ratio of 0.705 (Nasir *et al.* 1991); the protoliths were emplaced in an active continental margin at the Silurian–Devonian boundary (Okrusch & Richter 1986, Dombrowski *et al.* 1995).

The crystalline basement is unconformably overlain by Upper Permian (Zechstein) sedimentary strata (Figs. 1a, b, 2). These comprise a basal breccia and conglomerate, the Kupferschiefer and bituminous dolomites of the Werra Cycle, deposited in a marginal sea 258 – 256 Ma ago (German Stratigraphic Commission 2002). Compared to the dark gray, organic-matter-rich shales of the Kupferschiefer that were deposited in the deep marine basins of the Zechstein Sea under persistent euxinic conditions, the Kupferschiefer sedimentary sequence of the marginal facies is characterized by distinctly higher carbonate contents and a coarse lamination, reflecting a continuous variation between oxidizing and reducing (euxinic) conditions (*e.g.*, Paul 1982, Schumacher *et al.* 1984). A subsequent phase of erosion, testifying to a temporary regression of the Zechstein Sea, was followed by deposition of claystone and marlstone of the Leine(?) and Aller cycles (*e.g.*, Prüfert 1969, Paul 1982, 1985). These include the so-called Bröckelschiefer, formerly designated as being lowermost Triassic. The Upper Permian sedimentary rocks are overlain by sandy mudstone, sandstone and conglomeratic sandstone of the Lower Triassic (Buntsandstein). Both the crystalline basement and the post-Variscan sedimentary cover are cross-cut by predominantly SE-striking, steeply SW- or NE-dipping faults (Figs. 1a, 2), whereas NE-striking faults are subordinate (*e.g.*, Okrusch & Weinelt 1965). The boundary between the Spessart and the alluvial plain of the lower Main River coincides with a N–S- to NNW–SSE-striking normal fault with a downthrow of up to 500 m (*e.g.*, Okrusch *et al.* 1967). These fault systems were activated within the framework of the extensional tectonic regime that dominated central Europe in post-Variscan times (*e.g.*, Ziegler 1987).

Metallogenic framework

In the Spessart area, the Kupferschiefer and adjacent strata contain syngenetic to early diagenetic Pb–Zn–Cu(–Ag) mineralization with average metal grades of 1.80 wt.% Cu (range 0.21–4.50%), 0.17 wt.% Zn (range 0.03–0.35%) and 54 ppm Pb (range 13–145 ppm) (Schmitt 2001). Typical ore assemblages in the Huckelheim – Grosskahl area (Fig. 1a) are pyrite + tennantite in the Zechstein conglomerate, pyrite + marcasite + chalcopyrite + enargite + tennantite at the base of the Kupferschiefer, and galena + sphalerite + tennantite + löllingite in the upper parts of the Kupferschiefer and the overlying dolomites. Consequently, the Cu maximum is generally recorded in lower stratigraphic levels as compared to the Pb maximum (Schmitt 2001).

During a later, tectonically controlled phase of mineralization, the metal content of the Kupferschiefer was remobilized (Schmidt & Friedrich 1988, Vaughan *et al.* 1989, Schmidt *et al.* 1986). Hydrothermal fluids migrated along NE-striking faults and impregnated the basal Zechstein conglomerate, the Kupferschiefer itself and the lower part of the Werra dolomite with Cu–As–Ag–Pb–Zn minerals comprising tennantite, enargite, löllingite, siderite, chalcopyrite, galena and sphalerite as the main ore minerals (Schmitt 1992, 1993a, 2001; Fig. 1b). In addition, hydrothermal Ba–Co–Ni veins with tennantite, skutterudite, nickeline, arsenopyrite, chalcopyrite, barite and siderite were emplaced along NW-striking faults at Huckelheim (Schmitt 1993a). All these ores have been mined, with interruptions, between 1703 and 1837, in the "Segen Gottes" and "Hilfe Gottes" mines at Huckelheim and Grosskahl, respectively, with renewed mining activities between 1872 and 1918 proving futile (Freymann 1991). The Co–Ni–Bi vein deposits of the "Kobaltrücken" at Bieber (Figs. 1a, b), extensively mined between 1731 and 1869 (Freymann 1991, and references therein), are also related to the SE-striking fault system (Bücking 1892, Diederich & Laemmlen 1964). They contain skutterudite, diarsenides and sulfarsenides of a wide compositional range, as well as native bismuth as predominant ore minerals (Wagner & Lorenz 2002). In several places of the Spessart area, the NW–SE faults, cross-cutting the crystalline basement and the Permo-Triassic sedimentary cover, are invaded by barite veins (*e.g.*, Murawski 1954, Weinelt 1962, Hess 1973, Hofmann 1979), which locally contain fluorite (Okrusch & Weinelt 1965) or concentrations of Bi minerals, especially emplectite and native bismuth (Schmitt 1993b).

Stratabound Fe–Mn deposits occur within the Zechstein sediments, above the Kupferschiefer and below the Bröckelschiefer, at Bieber, Huckelheim, Sommerkahl and many other occurrences in the Spessart area

(Fig. 1b). They have been described previously (*e.g.*, Bücking 1892, Udluft 1923, Weidmann 1929) and were mined occasionally. Judging from their irregular distribution, their association with major faults and barite veins, and the silicification of associated dolomite, Okrusch & Weinelt (1965) proposed a hydrothermal–metasomatic origin for these deposits. This view has been confirmed by new observations indicating that, in places, the Zechstein dolomite is widely replaced by siderite and enriched in Ba, As and base metals, with Cu contents of up to 8400 ppm (Hartmann & Harris 1985, Schmitt & Lorenz, in prep.).

A complex assemblage of minerals, with Mn oxides, Mn carbonates, native arsenic, native bismuth and several accessory minerals, was recorded by Lorenz (1991, 1995, 2004) in a SE-striking fault zone that cuts a Lower Permian rhyolite near the village of Sailauf (Fig. 1b). The (U/Th)–He dating on the oxide minerals and K–Ar dating on illite (Hautmann *et al.* 1999, and pers. commun.) constrain the age of this mineralization. A pre-barite generation of braunite gave consistent (U/Th)–He dates of 158.0, 157.7 and 156.9 (± 4.8) Ma, whereas post-barite hematite was dated at 147.6 ± 4.5, 145.5 ± 5.7, 144.3 ± 4.4 and 136.3 ± 4.5 Ma; hausmannite yielded a (U/Th)–He age of about 130 Ma. The older (U/Th)–He dates were confirmed by conventional K–Ar dating on hydrothermal illite, which yielded 160.5 ± 4.5, 158.8 ± 3.0, 157.4 ± 3.2 and 156.4 ± 3.0 Ma, whereas younger K–Ar dates of 119.9 ± 5.7, 115.9 ± 5.6, 103.8 ± 1.5, 101.3 ± 4.4 and 98.2 ± 1.5 were recorded on various generations of celadonite. These results indicate an extended period of hydrothermal activity in the Spessart area, ranging from Middle Jurassic to Early Cretaceous time, presumably in different pulses.

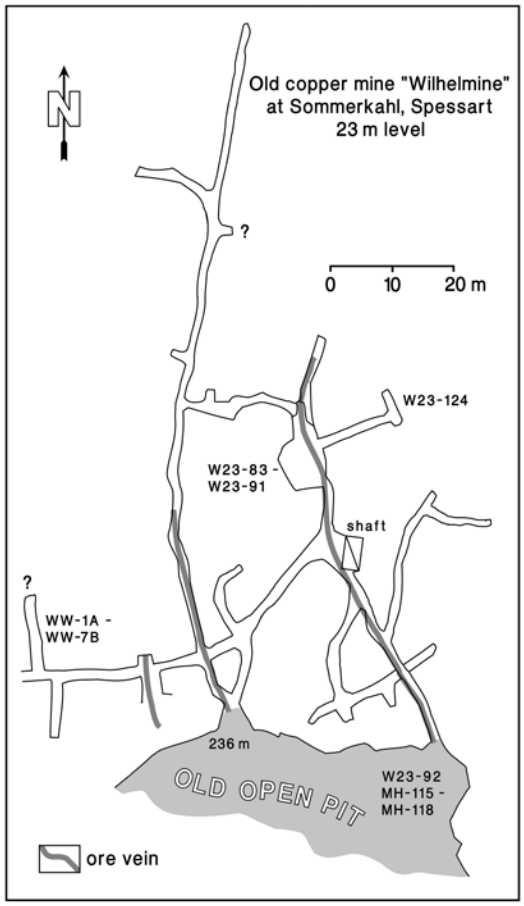

FIG. 3. The Wilhelmine mine at Sommerkahl. Ground plan of the 23 m level, surveyed by Bergtechnisches Vermessungsbüro Herbert Mathes & Söhne. Sample positions are indicated.

Mining area

The orthogneiss, exposed in the old open pit and the galleries of the underground mine (Fig. 3), displays a blastomylonitic flaser texture typical of the Rotgneiss Complex (Matthes & Okrusch 1965). Predominant minerals are quartz, K-feldspar (microcline microperthite), plagioclase ($An_{15–25}$), muscovite and biotite. Owing to hydrothermal alteration, which is not restricted to the sulfide veins but has affected wider parts of the Wilhelmine mine, biotite is totally replaced by fine-grained white mica + hematite. Along microfractures and grain boundaries, the gneiss is impregnated by fine-grained hematite. The orthogneiss is affected by strong post-mylonitic shearing (Okrusch & Weber 1996). Numerous fault-surfaces, in part listric, predominantly dip to the southeast; slickenside linears on these surfaces indicate that the dominant direction of transport of the upper block was toward the northeast.

The primary ore was concentrated in three SSE-striking fissure veins, attaining a maximum thickness of 20–30 cm, which were cut by steep E–W-striking faults (Okrusch & Weinelt 1965). In general, however, the ore invades cataclastic portions of the orthogneiss as an irregular network of anastomosing veinlets or stringers, ranging in diameter from a few centimeters to <0.1 mm. They cross-cut the schistosity under different angles and enclose fragments of the gneiss (Fig. 4a). Moreover, sulfide minerals are disseminated in portions of the gneiss.

Besides the ore veins, veins and fissure fillings of non-opaque minerals are also observed in the Wilhemine mine. Small crystals of quartz, up to 8 mm in size, commonly grow on the fracture faces of the gneiss, forming extensive mats of crystals. Ankerite and dolomite veins (up to 35 and 5 mm thick, respectively) may include some quartz, calcite and tennantite. Veinlets of barite, up to 5 mm thick, commonly overgrow crystals of dolomite and tennantite. From all these field

observations, the following paragenetic sequence of ore and gangue minerals can be deduced for the Wilhelmine mine: quartz → carbonates (dolomite, ankerite, calcite with rare inclusion of sulfides) → the main sulfide stage → barite (*cf.* Lorenz & Schmitt 2005).

Ore Petrography

The samples investigated

The clearing-up operations, necessary for setting up the visitors' mine, facilitated extensive sampling of the primary ore from a dump in the underground gallery at the 23 m level, in March 2002 (Fig. 3; samples W23–83 to W23–91 and W23–114). Samples WW–1 – WW–7 are from the 23 m level in the western part of the Wilhelmine mine, located in February 2003 (Fig. 3). Samples W23–92a, b, c and MHW–115 to MHW–118 were taken before 1970 from a rock face of the surface outcrop. A typical sample of the Wilhelmine ore is shown in Figure 4a.

Mineral assemblages

In all of the 26 samples from the Wilhelmine mine investigated by ore microscopy, tennantite is an important, in most cases predominant, constituent. It is generally accompanied by pyrite and chalcopyrite, which are absent only in a few samples (Table 1). Most of the ore samples from the 23 m level and from the open pit contain appreciable, in places dominant, bornite (Fig. 4a), generally together with digenite and, in some cases, enargite. In contrast, bornite and digenite are lacking in samples from the western part of the mine, many of which contain enargite instead. In most, though not all of the samples investigated, the copper sulfides are replaced by the "*blaubleibender covellin*" ("blue-remaining covellite") phases yarrowite and spionkopite, in part also by covellite proper. Additional secondary phases are goethite, malachite and rare marcasite. X-ray powder diffraction confirmed the presence of djurleite, anilite, azurite, native copper and jarosite in some of the samples. Veins predominantly consisting of gangue minerals like barite, ankerite, dolomite, calcite and quartz have also been recorded in the Wilhelmine mine. On the other hand, non-opaque minerals in the ore samples investigated are generally fragments of the hosting orthogneiss, and the only gangue mineral recorded is quartz.

Ore textures

On a microscopic scale, one can distinguish larger, though heterogeneous, veins of ore (a few millimeters to several centimeters across), from finer veinlets, which invade the gneiss along grain boundaries, cracks of individual grains and cleavage planes of micas (Fig. 5b). Ore minerals are also disseminated in the gneiss. Quartz grains, even those with undulatory extinction, do not show any sign of recrystallization in the vicinity of the ore veins. Textural evidence indicates that the ore-forming process took place in three different stages, namely (I) an early stage characterized by colloform textures, (II) a recrystallization stage, and (III) a late stage of alteration (Fig. 6).

At the *early stage I*, colloform textures are the most conspicuous characteristics of the Wilhelmine ore; they are present in virtually all samples (Figs. 4, 5; see also Freymann 1991, Fig. 4). They exhibit a considerable textural and mineralogical variety of spherical, cockade-like or garland-shaped monomineralic or polymineralic aggregates of pyrite I, tennantite I, bornite I, digenite I, chalcopyrite I, enargite I and quartz. These commonly form alternating zones in variable sequences, testifying to an oscillatory precipitation of the base-metal sulfides. Thus an unequivocal paragenetic succession of these stage-I minerals cannot be established (Fig. 6). Individual grains of pyrite are divided by thin gaps, suggestive of former syneresis cracks. Spherical, in part spherulitic aggregates of yarrowite – spionkopite – covellite were presumably formed by secondary alteration of some primary copper sulfide mineral(s).

During the *recrystallization stage II*, all these colloform textures were overgrown by, and enclosed in, anhedral bornite II, digenite II, enargite II, tennantite II, pyrite II, in places also by chalcopyrite II. Large grains of bornite II show exsolution lamellae of chalcopyrite IIa (W-type lamellae of Durazzo & Taylor 1982; see Figs. 4b, 5c). Tennantite II and digenite II overgrow

TABLE 1. ORE-MINERAL ASSEMBLAGES IN SAMPLES INVESTIGATED

	eng	tn	py	cpy	bn	dg/dju /ani	yar /spi	cv	mrc	gt	mal
W23-83	-	●	●	o	●	o	+	-	-	-	-
W23-84	-	●	o	o	o	-	o	-	-	o	o
W23-85	-	●	●	o	o	-	o	-	-	-	-
W23-86	-	●	●	+	o	o	-	-	-	o	-
W23-87	-	●	o	o	●	o	-	-	-	-	-
W23-88	-	●	o	+	o	o	+	-	-	-	+
W23-89a	o	●	●	o	o	o	-	-	o	-	-
W23-89b	o	●	o	o	●	o	-	-	-	-	-
W23-90	o	●	●	-	-	o	-	-	-	-	-
W23-91	-	o	o	+	●	-	●	-	-	-	-
W23-92a	-	o	o	o	●	o	+	-	-	-	-
W23-92b	-	o	o	o	●	o	+	-	-	-	-
W23-92c	-	●	o	o	●	o	+	-	-	-	-
W23-124	-	●	o	-	●	o	o	-	-	o	-
MHW-115	-	o	-	o	●	+	o	+	-	+	-
MHW-117	-	●	o	o	o	o	o	-	-	-	+
MHW-118	-	●	+	o	o	-	o	-	-	o	o
WW-1a	o	●	o	●	-	-	o	o	-	-	+
WW-1b	-	●	o	●	-	-	o	o	-	-	-
WW-1c	-	●	o	●	-	-	o	o	-	-	-
WW-2	+	●	o	o	-	-	o	o	-	-	-
WW-3	o	●	o	●	-	-	o	o	-	-	-
WW-4	-	●	o	o	-	-	-	-	-	-	-
WW-5	o	o	o	●	-	-	o	-	-	+	-
WW-6	o	o	●	o	-	-	o	o	-	-	-
WW-7a	o	●	o	o	-	-	-	-	-	-	-
WW-7b	o	●	o	o	-	-	-	-	-	-	+

Symbols: eng: enargite, tn: tennantite, py: pyrite, cpy: chalcopyrite, bn: bornite, dg: digenite, dju: djurleite, ani: anilite, yar: yarrowite, spi: spionkopite, cv: covellite, mrc: marcasite, gt: goethite, mal: malachite. Proportions of the minerals: ● >20 vol.%, o 20–1 vol.%, + <1 vol.%, - not recorded.

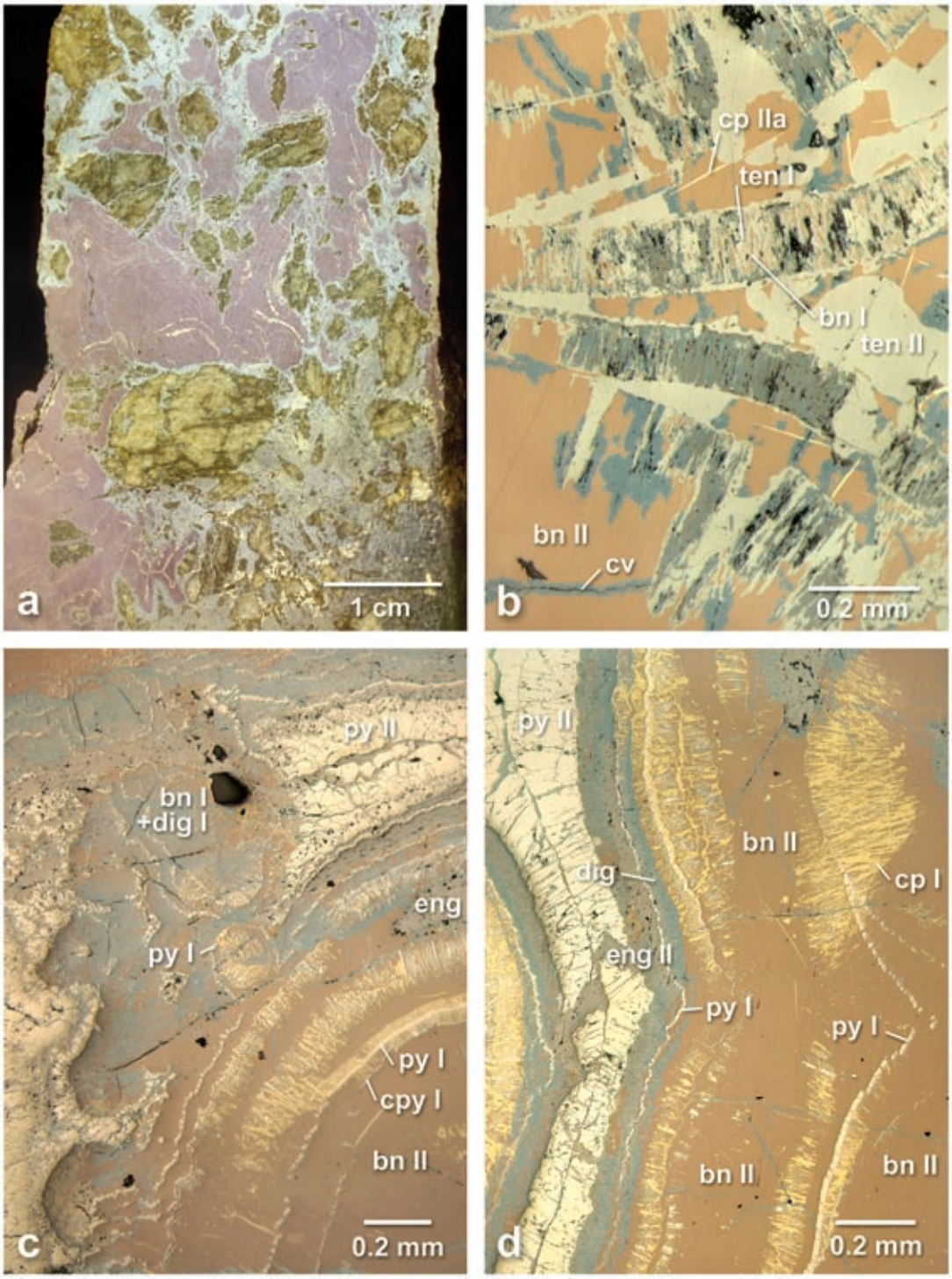
a
1 cm
b
cp IIa
ten I
bn I
ten II
bn II
cv
0.2 mm
c
py II
bn I
+dig I
eng
py I
py I
cpy I
bn II
0.2 mm
d
py II
bn II
dig
cp I
eng II
py I
py I
bn II
bn II
0.2 mm

or replace bornite II, chalcopyrite II and enargite II. In many cases, intimate, fine-grained intergrowths of digenite IIa and bornite IIa are observed (Fig. 5a), down to submicroscopic dimensions.

During the *late alteration stage III*, the primary sulfide minerals were replaced, along microfractures and grain boundaries, by yarrowite, spionkopite and rare covellite (Figs. 4b, 5b, c), together with products of weathering like goethite, malachite or jarosite. The alteration stage clearly postdates the exsolution of chalcopyrite IIa from bornite (Fig. 5c). Unfortunately, the characteristic textures indicative of replacement of the bornite by fine-grained aggregates of chalcopyrite, idaite and "*blaubleibender covellin*", described by Frenzel (1959, plate 4, Fig. 13; *cf.* von Gehlen 1964) in the Wilhelmine ore, have not been detected in the samples investigated.

Products of weathering

Recent weathering of the copper ores has led to the formation of a wealth of secondary minerals. In the open pit, these are mainly the carbonates malachite and azurite, and arsenates like olivenite, barium-pharmacosiderite, conichalcite and clinotyrolite. Sulfates like brochantite and langite were detected in the western part of the quarry, after the overburden was cleared away in 1981. In the underground workings, sulfates like gypsum, serpierite, orthoserpierite, brochantite and natrojarosite are predominant (Lorenz & Schmitt 2005).

FIG. 4. a) Hand-specimen photograph of a vein of copper ore from the Wilhelmine mine, with inclusions of brecciated orthogneiss. The predominant ore mineral is bornite, with subordinate tennantite, digenite and pyrite; garland- and cockade-shaped aggregates of pyrite indicate colloform textures of the early stage I. Collection of Werner Schaupert, Sommerkahl. b) – d) Photomicrographs showing textures of the Wilhelmine ore (uncrossed nicol). b) Curved, radiating aggregates of tennantite (ten) I + bornite (bn) I (+ secondary "*blaubleibender covellin*" phases + goethite); recrystallized grains of tennantite II and bornite II with rare unmixed chalcopyrite (cp) IIa; bornite is partly replaced by "*blaubleibender covellin*" phases (cv); sample MHW–115. c) Cockade-shaped aggregates of pyrite (py) I surrounding aggregates of bornite I + digenite I ± chalcopyrite I; garland-shaped aggregates of pyrite I; radial, garland-shaped aggregates of chalcopyrite I + pyrite I + bornite I; recrystallized pyrite II, bornite II and enargite II; sample W23–89a. d) Garland-shaped aggregates of pyrite I; radial, garland-shaped aggregates of chalcopyrite I + bornite I and of digenite + enargite I + pyrite I; recrystallized enargite II filling a crack in pyrite II; sample W23–89a.

ANALYTICAL METHODS

Analyses of the minerals

Electron-microprobe analyses were carried out using a CAMECA SX–50 electron-probe micro-analyzer (EPMA) equipped with three independent wavelength-dispersion spectrometers. Operating conditions were: 15 kV acceleration potential, 15 nA beam current, beam size 1 – 2 μm, integration time 20 s on TAP–PET and 30 s on LiF. The following standards and radiations were used: Se ($L\alpha$), Ag ($L\alpha$), Bi ($M\alpha$), Cu ($K\alpha$), Co ($K\alpha$), Ni ($K\alpha$), GaAs (As$L\alpha$), FeS_2 (Fe$K\alpha$, S$K\alpha$), ZnS (Zn$K\alpha$), Sb_2S_3 (Sb$L\alpha$), HgS (Hg$M\alpha$). Synthetic sulfides and pure elements were utilized for reference; matrix corrections were performed with the PAP program provided by CAMECA. Under these analytical conditions, the detection limit for the elements analyzed is 0.1 wt.%, and at best 0.05 wt.%; the analytical precision is about 1% for all major elements. Although the calculated formulae of minerals are satisfactory to good in most of the analyzed sulfide minerals, part of the analytical totals are somewhat high (especially for enargite, tennantite and "*blaubleibender covellin*" phases) or low (especially for bornite, chalcopyrite, digenite and pyrite). The total number of point analyses (n) carried out for each mineral or mineral group is given in brackets. Selected results of the electron-microprobe analyses are listed in Tables 2 to 9.

X-ray powder diffractometry

The samples were X-rayed using the automated powder diffractometer Philips PW1820 with Cu$K\alpha$ radiation and graphite monochromator. Data evaluation was performed by means of the Hanawalt Search Manual of the JCPDS file. The unit-cell parameters were calculated using the program EARLRAY (DOS version) designed by R. Haberkorn (Universität des Saarlandes, Saarbrücken, Germany).

Sulfur isotope analysis

In situ sulfur isotope measurements were performed on two or three spots of chalcopyrite, bornite, tennantite and enargite from the Wilhelmine samples WW–1a, W23–89b and W23–115 using the Finnigan–Neptune high-mass-resolution multicollector ICP–MS (Weyer & Schwieters 2003) combined with a Merchantek New Wave LUV 213 laser-ablation system. With this technique, the sulfur isotopes of sulfide minerals can be measured *in situ* in thick polished sections (> 100 μm). The method is described in more detail in Bendall *et al.* (2006). The amounts of ^{32}S and ^{34}S have been simultaneously measured with Faraday collectors. Since all S isotopes are affected by polyatomic mass interferences (if using a plasma source), measurements were performed in the Neptune high-resolution mode, which

TABLE 2. SELECTED COMPOSITIONS OF PYRITE

Sample	W23-89a							W23-91					WW-1a	
Point	A2	A4	A6	D1	D2	D6	D8	D4	D5	D6	D8	D14	B5	B7
Fe wt.%	45.79	46.12	46.65	45.47	45.21	45.55	45.47	45.68	46.40	46.21	46.01	44.84	44.99	44.92
Zn	0.05	0.05	<0.05	<0.05	<0.05	<0.05	0.07	<0.05	<0.05	<0.05	<0.05	0.07	<0.05	<0.05
Cu	0.20	0.20	0.10	1.05	0.68	0.53	0.59	0.14	0.32	0.33	0.36	0.53	0.36	0.20
Ag	<0.05	<0.05	0.16	<0.05	0.08	<0.05	0.06	0.07	<0.05	<0.05	<0.05	<0.05	<0.05	<0.05
Hg	<0.05	<0.05	<0.07	<0.05	0.14	<0.05	0.06	<0.05	<0.05	0.05	<0.05	0.05	<0.05	0.09
As	<0.05	<0.05	0.05	0.15	<0.05	0.10	<0.05	0.07	<0.05	<0.05	<0.05	0.18	<0.05	0.13
Sb	<0.05	<0.05	<0.05	0.21	0.18	0.08	<0.05	<0.05	<0.05	<0.05	<0.05	<0.05	<0.05	<0.05
Bi	0.16	0.15	0.25	<0.05	0.27	0.34	0.30	0.16	0.28	<0.05	0.25	0.08	0.17	0.30
S	53.11	53.31	53.07	53.47	53.10	52.75	52.98	52.73	53.27	53.60	53.80	52.82	53.09	52.73
Total	99.3	99.8	100.4	100.4	99.7	99.4	99.6	98.8	100.3	100.2	100.4	98.6	98.6	98.4
Fe *apfu*	0.992	0.994	0.989	0.976	0.979	0.989	0.985	0.995	0.998	0.991	0.985	0.978	0.979	0.982
Zn	-	0.001	-	-	-	-	0.001	-	-	-	-	0.001	-	-
Cu	0.004	0.004	0.002	0.020	0.013	0.010	0.011	0.003	0.006	0.006	0.007	0.010	0.007	0.004
Ag	-	-	0.002	-	0.001	-	0.001	0.001	-	-	-	-	-	-
Hg	-	-	-	-	0.001	-	-	-	-	-	-	-	-	0.001
As	-	-	0.001	0.002	0.002	0.002	0.002	0.001	-	-	-	0.003	-	0.002
Sb	-	-	-	0.002	0.002	0.001	-	-	-	-	-	-	-	-
Bi	0.001	0.001	0.002	-	0.002	0.001	0.002	0.001	0.002	-	0.002	-	0.001	0.002
Σ	0.997	1.000	0.996	1.000	0.998	1.004	1.000	1.001	1.006	0.997	0.994	0.992	0.987	0.991
S	2.004	2.000	2.004	1.999	2.002	1.995	1.999	2.000	1.995	2.002	2.007	2.007	2.013	2.009

Concentrations of Co, Ni and Se are less than 0.005%. The electron-microprobe data were converted to atoms per formula unit (*apfu*) on the basis of a total of three atoms.

is sufficient to resolve the major mass-interferences (*e.g.*, $^{16}O_2$ on ^{32}S, and $^{16}O^{18}O$ plus $^{16}O^{16}O^{1}H^{1}H$ on ^{34}S). We used laser parameters of 60 μm spot size, 10 Hz repetition rate, and a laser flux fluence of ~2.5 J/cm^2, which was sufficient to produce a signal of greater than 10 V (10^{-10} A) for ^{32}S for most sulfide minerals. We achieved "in run" precisions of <0.1‰ (1σ) for most measurements with this set-up.

The samples were measured relative to an in-house standard (a large crystal of pyrite from a massive sulfide deposit at Kambalda, Western Australia) with two measurements of the standard followed by 3–6 measurements on one sample, followed again by two measurements of the standard.

The in-house standard proved to be homogeneous during an earlier study (Bendall *et al.* 2006) within 0.32‰ (2σ) based on nine replicate LA–MC–ICP–MS measurements. In addition, it was calibrated by conventional gas spectrometry relative to the Canyon Diablo standard (Bendall *et al.* 2006). We used this calibration to recalculate the measured sulfur isotope compositions in this study as δ values relative to Canyon Diablo. External precision is probably mainly limited by sample heterogeneities. We expressed the uncertainty of the individual measurements of samples by using the 2σ uncertainty of the standard measurements before and after the respective measurements of the samples. The variation of replicate measurements in each grain is slightly larger, which might be due to S isotope heterogeneities within the grains. However, within the uncertainties of our method (given by the standard replicates), these variations within single grains could not be resolved.

Mineral Compositions

Pyrite

Pyrite ($n = 47$) is essentially stoichiometric, although minor amounts of Cu (up to 0.33 wt.% in recrystallized pyrite II and up to 1 wt.% in py I) and Bi (up to 0.35 wt.%) were detected, whereas Zn, Co, Ni, Ag, As, Sb, and Se are generally below or at the detection limit (Table 2). The highest values recorded are 0.23 wt.% Zn, 0.16% Ag, 0.24% Hg and 0.43% As. Analyses of fine-grained pyrite I showing Cu values well above 1 wt.% have been disregarded, since they are assumed to be influenced by secondary fluorescence of surrounding Cu minerals like tennantite or bornite.

Similar Cu contents of 0.11 to 0.90 wt.% were recorded by Schmitt (1991, 2001) in the various textural types of pyrite from the Zechstein conglomerate and the

Kupferschiefer at Grosskahl and Huckelheim, whereas Co, Ni, Zn and Ag in this pyrite are generally below the detection limit. In contrast, pyrite from Huckelheim shows generally higher As contents than those from the Wilhelmine ore, with up to 2.37 wt.% As in framboidal pyrite I and up to 1.36 wt.% As in anhedral pyrite II, whereas As in euhedral pyrite III is mostly below the detection limit.

Tennantite

EPMA datasets (n = 109), calculated to 16 cations, resulted in the following occupancies: $(Cu_{10.38–11.10}Fe_{0.11–0.93}Zn_{0.32–1.14}Co_{0.02–0.07})_{\Sigma 11.79–12.11}(As_{3.70–4.03}Sb_{0–0.15}Bi_{0–0.27})_{\Sigma 3.92–4.15}(S_{12.61–13.33}Se_{0–0.05})_{\Sigma 12.64–13.35}$, which closely approach the theoretical formula (Table 3, Fig. 7). With As/(As + Sb + Bi) atomic ratios of 0.92–0.99 (in 75 analyses, >0.98), tennantite is close to the As end member $Cu_{12}As_4S_{13}$. However, only in a few cases does the tennantite plot within the compositional field experimentally delineated by Maske & Skinner (1971) in the pure system Cu–As–S at temperatures of 300, 400 and 500°C (Fig. 7). Values of the atomic ratio Zn/(Zn + Fe) cover an extremely wide range, 0.27–0.90 (Fig. 8).

TABLE 3. SELECTED COMPOSITIONS OF TENNANTITE

Sample	W23-89a								W23-91	
Point	A5	A6	A7	A17	A20	D1	D9	D10	B2	C5
Cu wt.%	46.68	47.70	47.77	47.61	46.15	46.50	45.09	46.07	47.02	47.25
Ag	<0.05	<0.05	<0.05	0.06	<0.05	0.12	0.15	<0.05	0.09	<0.05
Hg	<0.05	0.08	0.12	0.17	<0.05	<0.05	<0.05	<0.05	<0.05	<0.05
Fe	3.29	1.79	1.50	2.00	2.83	1.41	2.53	1.28	1.35	2.02
Zn	1.53	2.51	2.19	2.24	2.17	3.68	2.61	4.16	3.38	2.43
Co	n.d.	n.d.	n.d.	n.d.	n.d.	0.13	0.23	0.10	0.18	0.14
As	20.21	19.78	20.28	19.65	19.72	19.82	19.08	19.54	20.10	19.93
Sb	0.27	0.17	0.24	0.36	0.32	0.64	0.55	0.55	0.25	0.11
Bi	0.21	0.30	0.42	0.20	1.00	0.52	2.45	0.41	0.39	0.61
S	28.36	28.48	28.22	28.18	28.23	27.88	27.76	28.08	28.26	28.08
Se	0.09	0.19	0.16	<0.05	0.13	0.08	0.16	0.08	<0.05	0.15
Total	100.6	100.9	100.8	100.4	100.6	100.8	100.6	100.4	101.0	100.7
Cu *apfu*	10.79	11.04	11.07	11.04	10.75	10.78	10.62	10.72	10.84	10.92
Ag	-	-	-	-	-	0.02	0.02	0.02	0.01	-
Hg	-	-	-	0.01	-	-	-	-	-	-
Fe	0.86	0.47	0.39	0.53	0.75	0.34	0.67	0.34	0.36	0.53
Zn	0.34	0.56	0.49	0.50	0.49	0.82	0.60	0.94	0.76	0.55
Co	-	-	-	-	-	0.03	0.06	0.03	0.05	0.03
Σ	11.99	12.07	11.95	12.08	11.99	11.99	11.95	12.05	12.02	12.03
As	3.96	3.88	3.99	3.86	3.90	3.90	3.80	3.86	3.93	3.91
Sb	0.03	0.02	0.03	0.04	0.04	0.08	0.07	0.07	0.03	0.01
Bi	0.01	0.02	0.03	0.01	0.07	0.04	0.17	0.03	0.03	0.04
Σ	4.00	3.92	4.05	3.91	3.99	4.02	4.04	3.96	3.99	3.96
S	12.99	13.06	12.96	12.94	13.03	12.80	12.95	12.95	12.91	12.87
Se	0.02	0.03	0.03	0.01	0.02	0.01	0.03	0.01	-	0.03
Σ	13.01	13.09	12.99	12.95	13.05	12.81	12.98	12.96	12.91	12.90

Concentrations of Ni are less than 0.05%. The electron-microprobe data were converted to atoms per formula unit (*apfu*) on the basis of a total of 16 atoms. n.d.: not determined.

Both Ag and Hg are generally below the detection limit, 0.1 wt.%, with maximum values of 0.22 wt.% Ag and 0.32 wt.% Hg. In contrast, nearly all point analyses reveal traces of Co, up to 0.30 wt.%, whereas Ni was never detected. In 63 point analyses, traces of Se (up to 0.27 wt.%) were found. No systematic compositional differences were recorded for the textural types tennantite I and tennantite II.

Compared to the Wilhelmine ores, tennantite from the Co–Ni–Bi vein mineralization at Bieber covers a distinctly wider range of Sb values, between 0.09 and 0.91 atoms per formula unit (*apfu*), and displays As/(As + Sb + Bi) values as low as 0.76, whereas the Zn/(Zn + Fe) atomic ratio shows a smaller variation, 0.19 to 0.38 (Wagner & Lorenz 2002; see Fig. 8). Moreover, tennantite from Bieber contains generally traces of Ag (up to 0.34 wt.%) and Hg (up to 0.65 wt.%), whereas tetrahedrite, filling late microfractures in the Bieber ore, is devoid of Ag and Hg.

Tennantite from Huckelheim displays a wide compositional range, with As/(As + Sb) values between 0.73 and 0.99, and Zn/(Zn + Fe) values between 0.17 and 0.87 (Fig. 8). Most of the tennantite in the lower parts of the Zechstein dolomites has Zn/(Zn + Fe) values less than 0.5, whereas in tennantite from the base of the Kupferschiefer and the Zechstein conglomerate, this ratio is greater than 0.5. Tennantite from the Kupferschiefer at Grosskahl shows similar As/(As + Sb) values, 0.72 to 0.93, but a distinctly smaller range in Zn/(Zn + Fe), between 0.21 and 0.43, which compares well with the tennantite at Bieber (Schmitt 1991, 2001). Like in the Bieber deposits, traces of Ag were recorded in tennantite from the Kupferschiefer at Grosskahl (up to 0.26 wt.%) and the dolomite of Huckelheim (up to 0.31 wt.%), whereas in tennantite from the Zechstein conglomerate and the Kupferschiefer at Huckelheim, Ag is generally below the detection limit. Virtually no Co and Ni was recorded in tennantite from Grosskahl and Huckelheim (Schmitt 1991, 2001).

Enargite

EPMA results on enargite (n =13) yielded a compositional range expressed by $Cu_{2.96–3.04}As_{0.98–1.02}S_{3.96–4.03}$, close to the theoretical formula (Table 4). Minor amounts of Bi and Fe are generally present, and reach maximum values of 0.28 and 0.37 wt.%, respectively, whereas Zn (up to 0.14 wt.%), Ag (up to 0.17 wt.%), Hg (up to 0.19 wt.%) and Se (up to 0.23 wt.%) were recorded in rare cases only; Co, Ni and Sb are below the detection limit.

With one exception, Fe contents in enargite from Grosskahl and Huckelheim are generally higher than in the Wilhelmine ore and range between 0.26 and 1.08 wt.%, whereas Ag and Zn are mostly below the detection limit (Schmitt 1991, 2001).

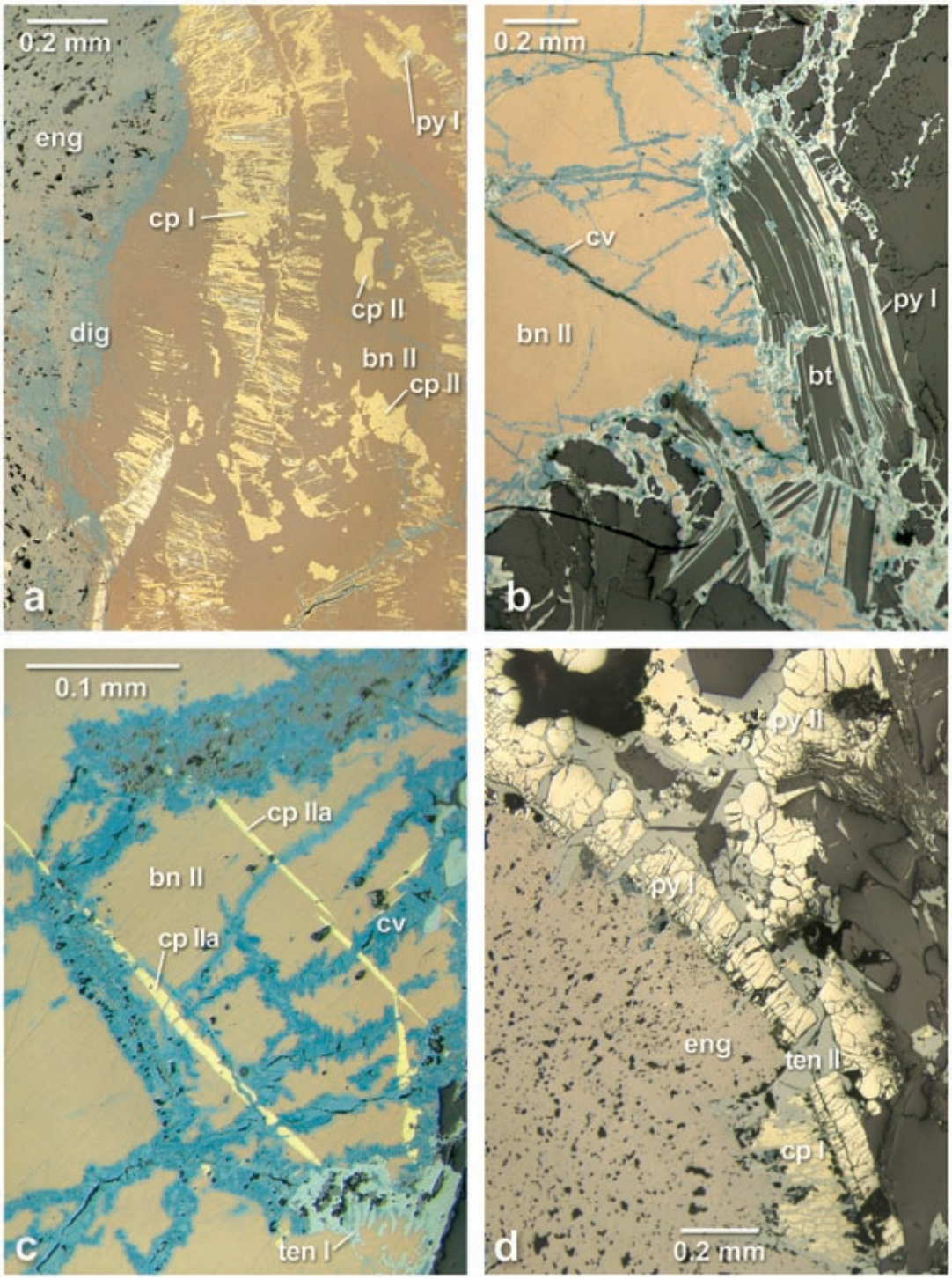
0.2 mm
eng
py I
cp I
cp II
dig
bn II
cp II
a
0.2 mm
cv
py I
bn II
bt
b
0.1 mm
cp IIa
bn II
cv
cp IIa
c
ten I
py II
py I
eng
ten II
cp I
d
0.2 mm

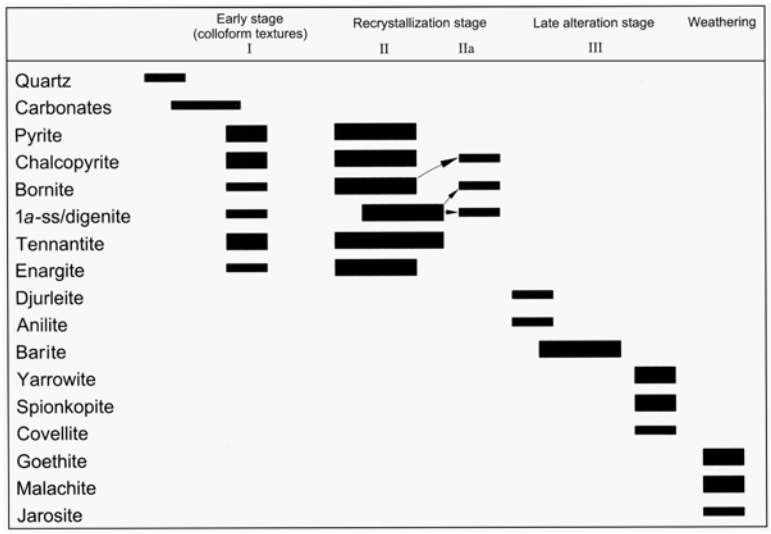

FIG. 6. Paragenetic sequence of the copper mineralization at Wilhelmine mine, as determined by textural evidence.

Chalcopyrite

EPMA results on chalcopyrite (n = 65) gave a compositional range expressed by $Cu_{0.98–1.10}Fe_{0.93–1.00}S_{1.97–2.03}$, close to the theoretical formula (Table 5, Fig. 9), although Fe/Cu values are below 1, with a minimum of 0.87. The only trace metal commonly recorded in chalcopyrite is Bi, with a maximum content of 0.30 wt.%. All other elements exceed the detection limit in a few cases only, with maximum values of 0.16 wt.% Zn, 0.15 wt.% Ag, 0.27 wt.% Hg and 0.13 wt.% of As, Sb and Se each. No systematic compositional differences have been detected between the three

FIG. 5. Photomicrographs showing structures of the Wilhelmine ore (uncrossed nicol). a) Garland-shaped aggregates of pyrite I; radial, garland-shaped aggregates of chalcopyrite I + subordinate pyrite I + bornite I; recrystallized enargite + digenite; blebs of chalcopyrite II and unmixing of chalcopyrite IIa (bottom, right) in bornite II; sample W23–89a. b) pyrite I and bornite I infiltrating biotite (bt), quartz and feldspars along cleavage planes and cracks; bornite II replaced by "*blaubleibender covellin*" phases along cracks; W23–91. c) Unmixing of chalcopyrite IIa from bornite II, which is replaced along cracks by "*blaubleibender covellin*" phases; bornite II overgrows tennantite I; sample MHW–115. d) Garland-shaped aggregate of pyrite I with dessication cracks, partly recrystallized and filled by tennantite II; aggregates of chalcopyrite I and tennantite I; intimate intergrowths of tennantite II and enargite II (left); sample WW–1a.

TABLE 4. SELECTED COMPOSITIONS OF ENARGITE

Sample	W23-89a		WW-1a			
Point	B1	C2	B2	B4	B5	B7
Cu wt.%	48.31	48.61	47.93	47.92	48.15	48.35
Fe	0.34	0.06	0.14	0.09	0.11	0.28
Zn	<0.05	0.14	<0.05	<0.05	<0.05	<0.05
Ni	<0.05	0.07	<0.05	<0.05	<0.05	<0.05
Ag	0.09	0.06	<0.05	<0.05	<0.05	<0.05
Hg	0.10	<0.05	0.19	<0.05	<0.05	<0.05
As	19.17	18.92	19.39	19.05	19.06	18.77
Sb	<0.05	<0.05	<0.05	<0.05	<0.05	0.05
Bi	0.16	0.16	<0.05	0.15	0.12	0.10
S	32.86	32.77	32.21	32.29	32.50	32.58
Se	0.23	0.07	0.15	0.10	0.10	0.15
Total	101.3	100.9	100.0	99.6	100.0	100.3
Cu *apfu*	2.964	2.991	2.983	2.988	2.987	2.991
Fe	0.024	0.004	0.010	0.006	0.008	0.020
Ni	-	0.005	-	-	-	-
Zn	-	0.008	-	-	-	-
Ag	0.003	0.002	-	-	-	-
Hg	0.002	-	0.004	-	-	-
Σ	2.993	3.010	2.997	2.994	2.995	3.011
As	0.997	0.988	1.023	1.007	1.002	0.985
Sb	-	-	-	-	-	0.002
Bi	0.003	0.003	-	0.002	0.002	0.002
Σ	1.000	0.991	1.023	1.009	1.004	0.989
S	3.995	3.996	3.973	3.990	3.995	3.994
Se	0.011	0.003	0.007	0.006	0.006	0.007
Σ	4.006	3.999	3.980	3.996	4.001	4.001

Concentrations of Co are less than 0.05%. The electron-microprobe data were converted to atoms per formula unit (*apfu*) on the basis of a total of eight atoms.

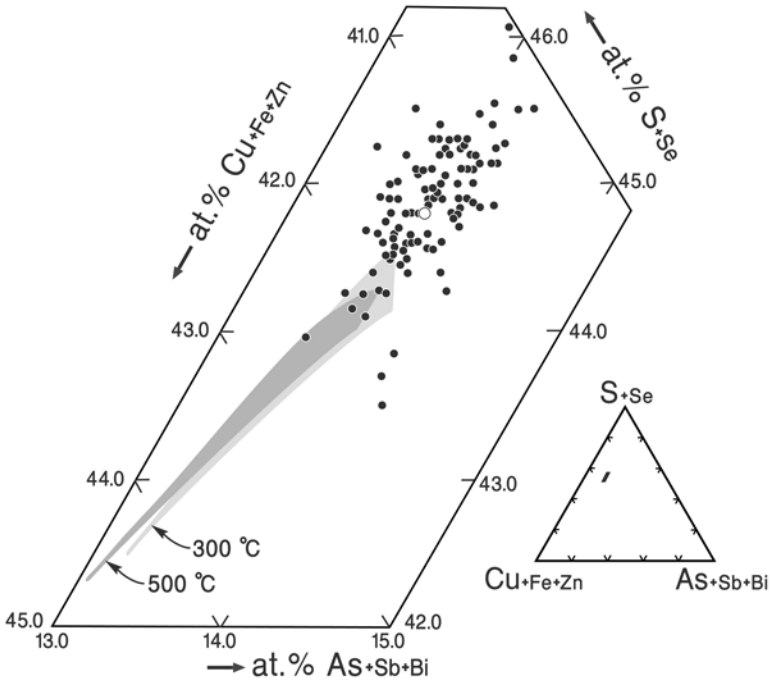

FIG. 7. EPMA point analyses of tennantite from the Wilhelmine mine plotted in part of the triangle Cu + Fe + Zn – As + Sb + Bi – S + Se. The ideal composition of tennantite, $Cu_{12}As_4S_{13}$, is indicated by an open circle; also given are the compositional fields of tennantite in the pure Cu – As – S system, experimentally determined by Maske & Skinner (1971) at 300 and 500°C.

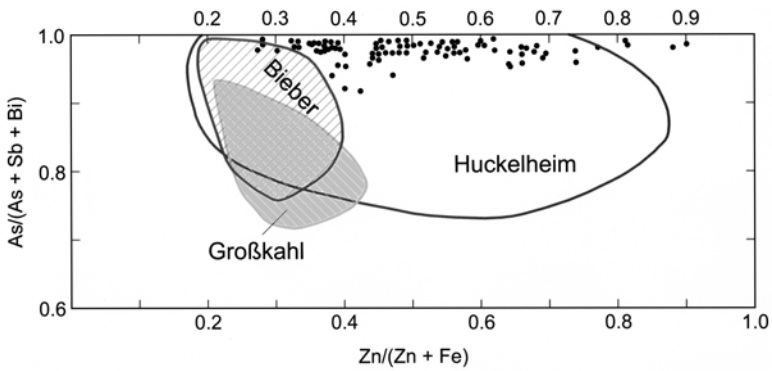

FIG. 8. EPMA point analyses of tennantite from the Wilhelmine mine in the diagram of atomic ratios Zn/(Zn + Fe) *versus* As/(As + Sb + Bi). The fields of tennantite compositions from Bieber (Wagner & Lorenz 2002), Grosskahl and Huckelheim (Schmitt 1993a) are delineated for comparison.

textural types of chalcopyrite. The assumption of von Gehlen (1964) that chalcopyrite IIa lamellae, exsolved from bornite, are not true $CuFeS_2$, but conform to a composition of about $Cu_5Fe_4S_{10}O_4$, was not substantiated by our analytical results.

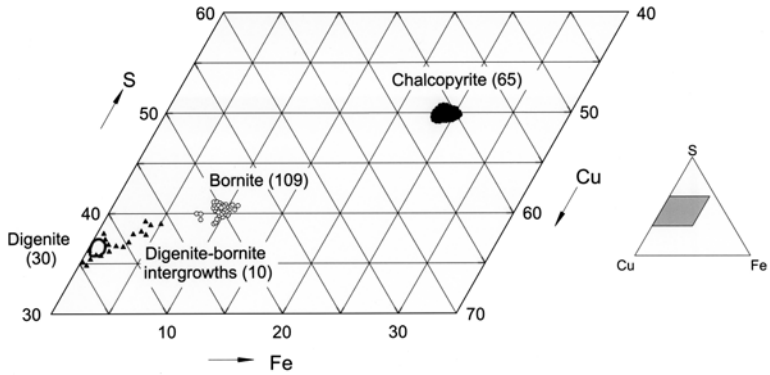

FIG. 9. Part of the triangle Cu – Fe – S showing the compositional fields of chalcopyrite (●), bornite (○) and digenite (delineated field, deviating point analyses and digenite–bornite intergrowths ▲); number of point analyses are given in brackets.

In chalcopyrite from Grosskahl and Huckelheim, Ag is invariably, and Zn generally, below the detection limit, whereas about half of the analyses revealed considerable As contents, up to 0.54 wt.% (Schmitt 1991, 2001).

Bornite

Orthorhombic, pseudo-tetragonal low bornite is the only polymorph known in nature (*e.g.*, Grguric *et al.* 2000). Accordingly, our calculated cell parameters, *a* 11.01(3), *b* 21.81(5) and *c* 10.88(6) Å, derived from powder-diffraction patterns, are similar to the values determined by Koto & Morimoto (1975). Close microscopic inspection, especially in oil immersion, revealed that bornite from the Wilhelmine mine is in fact anisotropic; large grains consist of lamellar intergrowths of two different varieties, with yellowish and bluish shades, respectively (*cf.* von Gehlen 1964). Nevertheless, nearly all point analyses (n = 109) define a limited range of composition, $Cu_{4.87–5.10}Fe_{0.92–1.11}S_{3.93–4.12}$, scattering around the theoretical formula Cu_5FeS_4 (Table 6, Fig. 9). Small amounts of Bi (up to 0.41 wt.%) and Ag (up to 0.38 wt.%) were recorded in 75 and 46 analyses, respectively. With rare exceptions, Zn (up to 0.16 wt.%), Hg (up to 0.34 wt.%), Co, Ni, As (up to 0.16 wt.% each), Sb (up to 0.14 wt.%) and Se (up to 0.14 wt.%) are at or below the detection limit of 0.1 wt.%.

Digenite

Cubic high digenite is stable above 82°C. In the system Cu – S, its composition varies between $Cu_{8.65}S_5$ and $Cu_{10}S_5$ (= $Cu_{1.75}S$ – Cu_2S; Roseboom 1966). However, in the system Cu – Fe – S, there is a broad solid-solution with bornite Cu_5FeS_4 at temperatures above 80°C, the so-called digenite-type or 1*a* solid-solution (Morimoto & Kullerud 1966, Morimoto & Gyobu 1971, Grguric *et al.* 2000), which becomes complete at the consolute point of 265°C (Grguric *et al.* 2000). Cubic low digenite *sensu stricto* has an integer 5*a* superstructure, which is metastable in the system Cu–S, but is stabilized by small amounts of Fe (Morimoto & Gyobu 1971). Natural low digenite shows a compositional range close to the Cu_9S_5–Cu_5FeS_4 join with 0.4–1.6 at.% Fe, corresponding to 4 to 16 mol.% of the bornite component, centered on a composition $Cu_{8.52}Fe_{0.12}S_{4.88}$ (= $Cu_{1.746}Fe_{0.025}S_1$) or 12 mol.% bornite (Morimoto & Gyobu 1971). According to *in situ* experiments of Grguric *et al.* (2000), low digenite$_{ss}$ may contain up to 19 mol.% of the bornite component at 25°C and up to ~25 mol.% at 80°C.

In the Wilhelmine ore, the presence of digenite was confirmed by X-ray powder diffraction, whereas the distinction from similar phases like anilite $Cu_{1.75}S$, djurleite $Cu_{1.96}S$ and chalcocite Cu_2S under the microscope is difficult and partly hampered by intimate intergrowths with bornite. In fact, in 10 out of 40 EPMA results with Fe contents between 1.9 and 5.1 at.%, corresponding to bornite contents of 27 to 55 mol.% (Figs. 9, 10), there are very fine-grained or submicroscopic digenite–bornite intergrowths, derived from unmixing of a 1*a* solid-solution. By contrast, 30 point analyses yielded lower Fe contents, in the range 0.18 to 1.03 at.%, *i.e.*, well below the upper limit for the Fe substitution in low digenite, with Cu/S values of 1.67 to 1.84 and Me^{tot}/S values of 1.70 to 1.85 (Table 7, Figs. 9, 10). Among these, in 17 datasets, the Cu/S values are between 1.73 and 1.84, well within the range of high digenite$_{ss}$, $Cu_{1.73–2.00}S$ (Roseboom 1966, Barton 1973), but only three datapoints are in the low digenite$_{ss}$ range, $Cu_{1.75–1.80}S$ (Morimoto & Koto 1970). We suspect that

TABLE 5. SELECTED COMPOSITIONS OF CHALCOPYRITE

Sample	W23-89a						W23-91	W23-92							MHW-115		WW-1a		
Point	B1 cpI	B6 cpI	B8 cpI	C2 cpI	C3 cpI	C6 cpI	C2 cpI	A4 cpI	A6 cpI	A7 cpI	A11 cpI	A14 cpI	B3 cpI	B6 cp1	A2 cpIII	B1 cpIII	A3 cpII	A4 cpII	B5 cpIII
Cu wt.%	35.10	35.10	34.93	35.04	36.44	35.00	35.72	35.26	35.63	36.00	34.53	35.12	35.43	35.36	35.54	35.42	34.32	34.16	34.51
Fe	29.38	29.66	29.85	29.31	28.84	29.20	27.98	28.90	28.28	28.34	29.96	29.35	29.05	29.03	29.29	27.87	29.67	29.76	28.24
Zn	<0.05	<0.05	<0.05	<0.05	<0.05	<0.05	<0.05	<0.05	0.06	0.10	<0.05	<0.05	<0.05	<0.05	<0.05	<0.05	<0.05	<0.05	<0.05
Ag	0.14	<0.05	<0.05	<0.05	0.10	0.14	0.09	<0.05	0.13	0.07	0.10	<0.05	<0.05	0.15	0.07	0.10	<0.05	<0.05	0.22
Hg	<0.05	<0.05	<0.05	0.18	0.11	0.12	<0.05	0.07	0.08	<0.05	<0.05	0.08	<0.05	0.09	0.11	0.27	<0.05	<0.05	<0.05
As	0.11	<0.05	0.06	0.10	<0.05	<0.05	<0.05	0.05	0.05	0.07	0.11	0.10	0.13	<0.05	<0.05	<0.05	<0.05	<0.05	<0.05
Sb	<0.05	<0.05	<0.05	<0.05	<0.05	0.06	<0.05	<0.05	<0.05	<0.05	0.10	0.13	<0.05	<0.05	<0.05	<0.05	<0.05	<0.05	<0.05
Bi	0.26	0.05	0.05	0.20	0.28	0.16	0.13	0.17	0.20	0.25	0.10	0.09	0.06	0.26	0.15	0.25	<0.05	0.13	0.25
S	34.65	34.83	35.09	34.66	34.08	35.30	34.68	35.08	35.27	35.48	35.12	34.71	34.60	34.74	35.07	35.10	35.29	34.56	34.87
Se	<0.05	<0.05	0.09	<0.05	<0.05	<0.05	<0.05	0.13	<0.05	<0.05	<0.05	<0.05	0.06	<0.05	<0.05	<0.05	<0.05	<0.05	<0.05
Total	99.64	99.72	100.07	99.49	99.85	99.98	98.60	99.66	99.65	100.31	100.02	99.58	99.33	99.63	100.23	99.01	99.28	98.61	99.09
Cu *apfu*	1.021	1.018	1.009	1.021	1.064	1.012	1.048	1.023	1.033	1.037	0.998	1.022	1.033	1.029	1.026	1.035	0.995	1.001	1.008
Fe	0.973	0.979	0.980	0.972	0.958	0.960	0.934	0.954	0.933	0.929	0.985	0.971	0.963	0.961	0.962	0.926	0.978	0.992	0.971
Zn	-	-	-	-	-	-	-	-	0.002	0.003	-	-	-	-	0.002	-	-	-	-
Ag	0.002	-	-	-	0.002	0.002	0.002	-	0.002	0.001	0.002	-	-	0.003	0.001	0.002	-	-	-
Hg	-	-	-	0.002	0.001	0.001	-	0.001	0.001	-	-	0.001	-	0.001	0.001	0.002	-	0.002	-
As	0.003	-	0.002	0.002	-	-	-	0.001	-	0.002	0.003	0.002	0.003	-	-	-	-	-	-
Sb	-	-	-	-	-	0.001	-	-	-	-	0.002	0.002	-	-	-	-	-	-	-
Bi	0.002	-	-	0.002	0.002	0.002	0.001	0.002	0.002	0.002	0.001	0.001	-	0.002	0.001	0.002	-	0.001	0.002
Σ	2.001	1.997	1.991	1.999	2.027	1.978	1.985	1.981	1.973	1.974	1.991	1.999	1.999	1.996	1.993	1.967	1.973	1.994	1.983
S	1.998	2.002	2.007	2.001	1.972	2.022	2.016	2.017	2.027	2.026	2.010	2.001	1.999	2.004	2.007	2.032	2.026	2.006	2.017
Se	-	-	0.002	-	-	-	-	0.003	-	-	-	-	0.001	-	-	-	-	-	-
Σ	1.998	2.002	2.009	2.001	1.972	2.022	2.016	2.020	2.027	2.026	2.010	2.001	2.000	2.004	2.007	2.032	2.026	2.006	2.017

Concentrations of Co and Ni are less than 0.05%. The electron-microprobe data were converted to atoms per formula unit (*apfu*) on the basis of a total of four atoms.

natural, low-temperature leaching of metal, described by Goble (1981), is responsible for the Cu deficiencies in some of the digenite grains analyzed.

With two exceptions, EPMA of digenite yielded considerable Ag contents, up to 1.52 wt.%, the highest Ag value recorded in the sulfide minerals of the Wilhelmine mine. Traces of Bi (up to 0.29 wt.%) were recorded in more than half of the analyses, whereas Hg exceeds the detection limit in a few cases only (up to 0.31 wt.%). Furthermore, Zn, Co, Ni, As (with one exception: 0.20 wt.%), Sb and Se are at or below the detection limit of 0.1 wt.%.

Djurleite and anilite

The stable low-temperature copper sulfide phases djurleite $Cu_{1.93–1.96}S$ (stable at <93°C; Roseboom 1962, Morimoto 1962, Potter 1977) and anilite $Cu_{1.75}S$ (stable at <75°C; Morimoto *et al.* 1969, Morimoto & Koto 1970) were identified in two samples from the Wilhelmine mine, by X-ray powder diffractometry. *Anilite* in sample W23–100, from the 23 m level, forms tiny crystals together with quartz and traces of bornite and is overgrown by malachite (Lorenz & Schmitt 2005). Euhedral crystals of *djurleite* occur in the western part of the mine, filling lensoid fissures together with predominant tennantite and digenite and minor kaolinite (sample W23–112). Unit-cell parameters calculated from powder-diffraction patterns compare well with literature data (Koto & Morimoto 1970, Evans 1979): anilite: *a* 7.878(5), *b* 7.839(6), *c* 11.058(7) Å; djurleite: *a* 26.89(1), *b*15.726(9), *c* 13.48(1) Å, β 90.01(8)°.

Electron-microprobe analyses on polished grain mounts of an *anilite* concentrate from sample W23–100 (n = 12) yielded compositions between $Cu_{1.69}S$ and $Cu_{1.77}S$ (average $Cu_{1.72}S$), which is close to the ideal formula (Table 8). Some of the point analyses revealed traces of Bi (up to 0.21 wt.%), Hg (up to 0.16 wt.%), Ag (up to 0.13 wt.%), Fe (up to 0.12 wt.%) or Se (up to 0.11 wt.%), whereas Zn, Co, Ni, As and Sb are invariably at or below the detection limit.

TABLE 6. SELECTED COMPOSITIONS OF BORNITE

Sample	W23-87		W23-89a					W23-91		W23-92					MHW-115		
Point	A2	A8	B15	B16	B22	C4	C10	A5	C4	A7	A21	A22	B5	B6	A4	B4	B7
Cu wt.%	63.08	63.12	63.44	63.45	62.76	63.19	63.52	63.35	62.93	63.18	62.09	62.30	63.08	63.07	62.46	63.21	62.61
Fe	10.82	10.41	10.80	10.84	10.76	11.11	10.88	10.57	10.78	10.86	10.77	10.98	10.70	10.75	11.04	10.65	10.82
Zn	<0.05	<0.05	<0.05	<0.05	<0.05	<0.05	<0.05	<0.05	0.16	<0.05	<0.05	<0.05	<0.05	<0.05	<0.05	0.08	<0.05
Ag	0.13	0.20	<0.05	0.19	0.10	<0.05	0.19	0.05	<0.05	0.11	0.15	<0.05	0.14	0.13	0.14	0.09	0.08
Hg	<0.05	0.06	<0.05	0.16	0.07	<0.05	<0.05	0.15	<0.05	0.15	<0.05	<0.05	0.29	0.11	<0.05	0.08	<0.05
As	0.06	<0.05	<0.05	<0.05	<0.05	0.06	0.09	<0.05	<0.05	<0.05	<0.05	0.09	0.16	<0.05	<0.05	<0.05	0.06
Sb	0.07	<0.05	<0.05	<0.05	<0.05	<0.05	<0.05	<0.05	<0.05	<0.05	<0.05	<0.05	<0.05	0.07	<0.05	0.05	0.08
Bi	0.06	0.27	0.16	0.15	<0.05	0.24	<0.05	0.18	0.19	0.07	0.13	0.13	0.10	0.17	0.23	<0.05	0.12
S	25.87	25.65	25.91	25.71	25.65	25.50	25.84	25.64	25.81	25.59	25.87	26.28	24.28	24.97	25.67	25.78	25.86
Se	<0.05	0.06	<0.05	<0.05	<0.05	0.11	<0.05	<0.05	<0.05	<0.05	<0.05	0.11	<0.05	<0.05	<0.05	<0.05	0.05
Total	100.09	99.77	100.31	100.50	99.34	100.21	100.52	99.94	100.10	99.96	99.01	99.89	98.75	99.27	99.54	99.94	99.68
Cu *apfu*	4.974	5.007	4.991	4.999	4.985	4.994	4.990	5.016	4.954	4.999	4.938	4.903	5.100	5.046	4.955	4.994	4.954
Fe	0.970	0.939	0.966	0.971	0.972	0.999	0.972	0.952	0.966	0.977	0.974	0.983	0.984	0.979	0.996	0.957	0.974
Zn	-	-	-	-	-	-	-	0.012	-	-	-	-	-	-	0.006	-	
Ag	0.006	0.009	-	0.009	0.005	-	0.009	0.002	-	0.005	0.007	-	0.006	0.006	0.006	0.004	0.004
Hg	-	0.001	-	0.004	0.002	-	-	0.004	-	0.004	-	-	0.007	0.003	-	0.002	-
As	0.004	-	-	-	-	-	0.006	-	-	-	-	0.006	0.011	-	-	-	0.004
Sb	0.003	-	-	-	-	-	-	-	-	-	-	-	-	0.003	-	0.002	0.003
Bi	0.001	0.006	0.004	0.004	-	0.006	-	0.004	0.005	0.002	0.003	0.003	0.003	0.004	0.006	-	0.003
Σ	5.958	5.962	5.961	5.987	5.964	5.999	5.977	5.978	5.937	5.987	5.922	5.895	6.111	6.041	5.963	5.965	5.942
S	4.042	4.032	4.039	4.013	4.036	3.993	4.023	4.022	4.063	4.012	4.077	4.099	3.889	3.959	4.036	4.035	4.055
Se	-	0.004	-	-	-	0.007	-	-	-	-	-	0.007	-	-	-	-	0.003
Σ	4.042	4.036	4.039	4.013	4.036	4.000	4.023	4.022	4.063	4.012	4.077	4.106	3.889	3.959	4.036	4.035	4.058

Concentrations of Co and Ni are less than 0.05%. The electron-microprobe data were converted to atoms per formula unit (*apfu*) on the basis of a total of ten atoms.

TABLE 7. SELECTED COMPOSITIONS OF DIGENITE

Sample	W23-83		W23-87				W23-89a				W23-92
Point	A11	A13	A2	A4	A6	A12	B8	B9	B11	B21	C1
Cu wt.%	75.24	75.25	76.05	76.35	75.43	76.28	76.42	75.78	76.21	78.66	75.22
Fe	0.56	0.40	0.83	0.46	0.40	0.53	0.41	0.81	1.03	0.28	0.63
Zn	<0.05	<0.05	<0.05	<0.05	<0.05	0.09	<0.05	<0.05	<0.05	0.06	<0.05
Ag	0.52	0.57	0.32	0.14	0.21	0.36	0.54	0.08	0.15	0.23	<0.05
Hg	<0.05	0.31	<0.05	0.26	<0.05	<0.05	0.12	<0.05	<0.05	<0.05	<0.05
Ni	<0.05	<0.05	<0.05	<0.05	<0.05	0.07	n.d	n.d.	n.d	n.d.	n.d.
As	<0.05	<0.05	<0.05	<0.05	<0.05	0.06	<0.05	<0.05	<0.05	<0.05	<0.05
Bi	0.22	<0.05	0.10	<0.05	0.19	0.11	0.21	0.17	<0.05	<0.05	0.29
S	21.89	21.98	22.18	22.23	22.11	22.17	21.50	22.75	23.15	21.54	22.47
Se	<0.05	<0.05	<0.05	<0.05	<0.05	0.11	0.09	<0.05	<0.05	0.05	<0.05
Total	98.43	98.51	99.48	99.44	98.43	99.69	99.28	99.65	100.54	100.82	98.66
Cu *apfu*	1.735	1.728	1.730	1.733	1.721	1.733	1.791	1.681	1.706	1.843	1.689
Fe	0.015	0.010	0.022	0.012	0.010	0.014	0.011	0.021	0.025	0.007	0.016
Zn	-	-	-	-	0.002	-	-	-	-	0.001	-
Ag	0.007	0.008	0.004	0.002	0.003	0.005	0.007	0.001	0.002	0.003	-
Ni	-	-	-	-	-	0.002	-	-	-	-	-
As	-	-	-	-	-	0.001	-	-	-	-	-
Bi	0.002	-	0.001	-	0.001	0.001	0.002	0.001	-	-	0.002
Σ	1.759	1.748	1.757	1.749	1.737	1.733	1.812	1.705	1.733	1.845	1.707
S	1.000	1.000	1.000	1.000	1.000	0.998	0.998	1.000	1.000	1.000	1.000
Se	-	-	-	-	-	0.002	0.002	-	-	-	-
Σ	1.000	1.000	1.000	1.000	1.000	1.000	1.000	1.000	1.000	1.000	1.000

Concentrations of Co and Sb are less than 0.05%. The electron-microprobe data were converted to atoms per formula unit (*apfu*) on the basis of a total of (S + Se) equal to one.

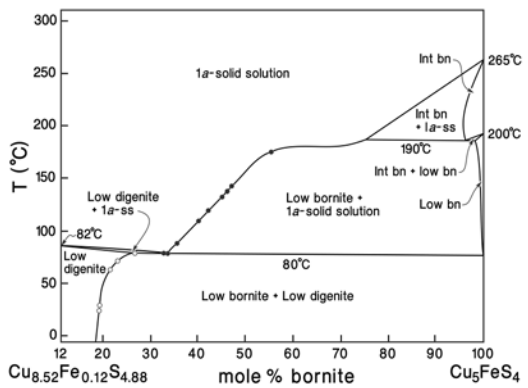

FIG. 10. Phase diagram for the condensed phases in the bornite–digenite series after Grguric *et al.* (2000). Indicated are results of electron-microprobe analyses of fine-grained ("spotty") or submicroscopic aggregates of digenite + bornite representing the composition of a former 1*a* solid-solution (●) and of digenite coexisting with bornite representing the low bornite – low digenite solvus (○).

Djurleite in grain-mount sample W23–112 (n = 2) gave a formula of $Cu_{1.85}S$ (Table 8), *i.e.*, its Cu:S ratio is distinctly below the compositional range of $Cu_{1.93–1.97}S$ so far known for djurleite, but above the range of digenite compositions $Cu_{1.75–1.80}S$ (Goble 1981, Table 1). Traces of Fe (up to 0.13 wt.%) and Bi (up to 0.14 wt.%) were recorded, whereas all other metals are at or below the detection limit.

It cannot be excluded that digenite–bornite intergrowths in the Wilhelmine ore contain some anilite; compositions close to djurleite have not been recorded in these intergrowths.

Yarrowite, spionkopite and geerite(?)

Covellite from the Wilhelmine mine has been already described by Fritz (1895), using the traditional German term "Kupferindig", and was also mentioned by Okrusch & Weinelt (1965). However, most of the covellite-like phases replacing the primary sulfide minerals are in fact "*blaubleibender covellin*", first recognized by Frenzel (1959) in copper ores from various localities. Among these, he described an ore sample from Sommerkahl, in which bornite is replaced by fine-grained aggregates of "*blaubleibender covellin*", idaite

and chalcopyrite. Extensive electron-microprobe work of Goble & Smith (1973) showed that "*blaubleibender covellin*" consists in fact of two hexagonal phases, namely $Cu_{1.32\pm0.04}S$ and $Cu_{1.12\pm0.05}S$, which were later on named spionkopite and yarrowite, respectively (Goble 1980). In addition, Goble & Robinson (1980) detected a third pseudocubic copper sulfide phase, geerite, with a compositional range of $Cu_{1.5}S$ – $Cu_{1.6}S$ (Goble 1981, Table 1).

Three samples of Wilhelmine ore, containing relatively coarse-grained vein fillings of "*blaubleibender covellin*", indeed yielded three groups of the following compositional ranges (Table 9): (i) $Cu_{1.10}S$ – $Cu_{1.19}S$, with an average of $Cu_{1.12}S$, corresponding to *yarrowite*, were predominantly recorded in samples W23–91 (n = 12) and W 23–115 (n = 14). Zinc, Co, Ni, As, Sb and Se are below the detection limit, whereas about half of the compositions reveal traces of Ag (up to 0.27 wt.%) and Bi (up to 0.26 wt.%); in rare cases, Hg (up to 0.27 wt.%) was recorded. Yarrowite in sample W23–91 contains 0.13–0.66 wt.% Fe, whereas in sample W23–115, a measurable Fe content (0.60 wt.%) was obtained in only one case. (ii) Nearly all point analyses in sample W23–92 (n = 9), but only three in sample W23–91 and –115 yielded a compositional range of $Cu_{1.21}S$ – $Cu_{1.33}S$, overlapping, but not identical with, the range of *spionkopite* compositions described in the literature (Goble 1981, Table 1), the average value being at $Cu_{1.27}S$. Spionkopite from the Wilhelmine mine invariably contains some Ag (0.25–0.55 wt.%), whereas Fe (up to 1.01 wt.%) and Bi (up to 0.28 wt.%) were recorded only in eight and seven analyses, respectively. Mercury (with one exception: 0.14 wt.%), Zn, Co, Ni, As, Sb and Se are below the detection limit. (iii) Four point-analyses of "*blaubleibender covellin*" in sample W23–115 revealed $Cu_{1.49}S$ to $Cu_{1.53}S$, on average $Cu_{1.52}S$, which is at the lower end of the compositional range of geerite (a fifth sample with $Cu_{1.42}S$ was excluded). Bi (up to 0.22 wt.%) was recorded in nearly all analyses, and Ag (up to 0.24 wt.%) in about half of the analyses, whereas Fe, Zn, Hg, Co, Ni, As, Sb and Se are below the detection limit. So far, the presence of geerite has not been confirmed by X-ray diffractometry.

TABLE 8. SELECTED COMPOSITIONS OF DJURLEITE AND ANILITE

Mineral	djurleite		anilite					
Sample	W23-112		W23-110					
Point	A1	A2	A2	A3	A4	A5	A10	A11
Cu wt.%	77.80	77.98	77.49	77.01	76.98	77.33	77.14	77.38
Fe	0.13	0.13	<0.05	0.12	0.13	<0.05	<0.05	<0.05
Zn	<0.05	0.07	<0.05	0.06	<0.05	<0.05	<0.05	<0.05
Ag	<0.05	<0.05	0.13	<0.05	<0.05	<0.05	<0.05	<0.05
Hg	<0.05	<0.05	0.16	<0.05	0.10	<0.05	0.12	<0.05
Ni	<0.05	<0.05	<0.05	<0.05	<0.05	<0.05	<0.05	0.10
As	<0.05	<0.05	0.06	<0.05	<0.05	<0.05	<0.05	<0.05
Sb	<0.05	0.06	<0.05	<0.05	<0.05	<0.05	<0.05	<0.05
Bi	0.14	0.06	<0.05	<0.05	<0.05	0.08	0.16	<0.05
S	21.22	21.22	22.07	22.42	22.67	22.14	22.63	22.60
Se	0.08	<0.05	<0.05	<0.05	<0.05	0.06	<0.05	<0.05
Total	99.37	99.52	99.91	99.61	99.88	99.61	100.05	100.08
Cu *apfu*	1.848	1.855	1.771	1.734	1.714	1.761	1.721	1.728
Fe	0.003	0.003	-	0.003	0.003	-	-	-
Zn	-	0.002	-	0.001	-	-	-	-
Ag	-	-	0.002	-	-	-	-	-
Hg	-	-	0.001	-	0.001	-	0.001	-
Ni	-	-	-	-	-	-	-	0.002
As	-	-	0.001	-	-	-	-	-
Sb	-	0.001	-	-	-	-	-	-
Bi	0.001	-	-	-	-	-	0.001	-
Σ	1.852	1.861	1.775	1.738	1.718	1.761	1.723	1.730
S	1.000	1.000	1.000	0.999	1.000	1.000	1.000	1.000
Se	-	-	-	0.001	-	-	-	-
Σ	1.000	1.000	1.000	1.000	1.000	1.000	1.000	1.000

Concentrations of Co are less than 0.05%. The electron-microprobe data were converted to atoms per formula unit (*apfu*) on the basis of a total of (S + Se) equal to one.

Covellite

True covellite showing the typical color-change in oil immersion was rarely encountered in the Wilhelmine ore. Five point-analyses on a covellite flake in sample W23–115 led to the compositional range $Cu_{1.05}S$ – $Cu_{1.07}S$ (Table 9), which is close to, but not identical with, the theoretical formula CuS (Goble 1981, Table 1). In addition, 0.13–0.38 wt.% Fe and 0.19 – 0.24 wt.% Ag were recorded, whereas Zn (up to 0.15 wt.%), Bi (up to 0.20 wt.%) and Se (up to 0.12 wt.%) are mostly below the detection limit, and Hg, Co, Ni, As and Sb, always so.

Sulfur Isotopes

Earlier sulfur isotope analyses, performed by Paula Hahn-Weinheimer, Munich, on one sulfide-bearing quartz–barite vein and four samples of sulfide-impregnated gneiss from the Wilhelmine mine yielded $\delta^{34}S$ values of –18.6, –20.9, –22.4, –22.7 and –24.6‰ (Okrusch & Weinelt 1965).

Unfortunately, neither a detailed description of the analyzed samples nor the analytical details and uncertainties of her data were given by the authors. In order to test these results, we performed *in situ* sulfur isotope measurements on coexisting sulfide minerals in three Wilhelmine samples, using a LA–Multicollector ICP–MS instrument. Only sulfide grains formed during the recrystallization stage II were sufficiently large to avoid "composite" analyses of different intergrown sulfide phases. Our analyses yielded distinctly negative $\delta^{34}S$ values ranging from –12.8 to –23.9‰ (Table 10), thus broadly confirming the earlier data of Hahn-Weinheimer. There are considerable differences among the three samples investigated, whereas different minerals in the same sample gave similar $\delta^{34}S$ values, with differences in the isotopes close to the analytical uncertainties of ~ 1‰. For instance, the

TABLE 9. SELECTED COMPOSITIONS OF COVELLITE, YARROWITE, SPIONKOPITE AND GEERITE (?)

Mineral	covellite		yarrowite						spionkopite					geerite (?)	
Sample	W23-115		W23-91		W23-92	W23-115			W23-92			W23-115		W23-115	
Point	C11	C15	B1	B5	A2	C2	C6	C18	A1	A6	A7	A10	C2	C6	C7
Cu wt.%	67.68	67.09	67.90	67.97	68.62	69.82	68.86	68.55	71.45	70.19	70.41	71.44	70.62	74.92	74.60
Fe	0.28	0.47	0.58	0.66	<0.05	<0.05	<0.05	0.60	0.14	<0.05	0.18	0.53	0.47	0.09	0.08
Zn	<0.05	<0.05	<0.05	<0.05	<0.05	<0.05	<0.05	<0.05	<0.05	<0.05	<0.05	0.08	0.05	<0.05	<0.05
Ag	0.19	0.28	<0.05	0.14	0.22	0.12	0.12	<0.05	0.32	0.73	0.25	0.30	0.21	0.09	0.21
Hg	<0.05	0.15	<0.05	0.08	<0.05	<0.05	<0.05	<0.05	<0.05	<0.05	<0.05	<0.05	0.06	<0.05	<0.05
Sb	<0.05	<0.05	0.10	<0.05	<0.05	<0.05	<0.05	<0.05	<0.05	0.07	<0.05	<0.05	<0.05	<0.05	<0.05
Bi	0.20	0.05	0.15	0.10	<0.05	0.22	<0.05	<0.05	0.18	0.21	0.21	0.19	0.28	0.18	0.06
S	32.53	32.03	31.57	31.27	29.68	30.68	31.07	30.97	28.36	28.36	28.74	27.17	28.05	24.74	24.84
Se	<0.05	<0.05	0.06	<0.05	0.07	<0.05	0.10	<0.05	<0.05	0.09	<0.05	<0.05	0.08	<0.05	<0.05
Total	100.88	100.07	100.46	100.22	98.73	99.64	100.20	100.17	100.45	99.65	99.79	99.67	99.82	100.02	99.79
Cu	1.050	1.057	1.085	1.097	1.167	1.128	1.118	1.117	1.272	1.249	1.236	1.326	1.269	1.528	1.516
Fe	0.005	0.008	0.010	0.012	0.001	-	-	0.001	0.003-	0.004	0.011	0.010	0.002	0.002	
Zn	-	-	-	-	-		-	-	-	-	-	0.001	0.001	-	-
Ag	0.002	0.003	-	0.001	0.002	0.001	0.001	-	0.003	0.008	0.003	0.003	0.002	0.001	0.003
Hg	-	0.001	-	-	-	-	-	-	-	-	-	-	-	-	-
Sb	-	-	0.001	-	-	-	0.001	-	-	-	-	-	-	-	-
Bi	0.001-	-	0.001	-	-	0.001	-	-	0.001	0.001	0.001	0.001	0.002	0.001	-
Σ	1.057	1.069	1.097	1.110	1.170	1.130	1.120	1.119	1.279	1.259	1.244	1.342	1.282	1.532	1.521
S	1.000	1.000	1.000	1.000	0.999	1.000	0.999	1.000	1.000	0.999	1.000	1.000	0.999	1.000	1.000
Se	-	-	-	-	0.001	-	0.001	-	-	0.001	-	-	0.001	-	-
Σ	1.000	1.000	1.000	1.000	1.000	1.000	1.000	1.000	1.000	1.000	1.000	1.000	1.000	1.000	1.000

Concentrations of Co, Ni and As are less than 0.05%. The electron-microprobe data were converted to atoms per formula unit (*apfu*) on the basis of a total of (S + Se) equal to one.

average $\delta^{34}S$ values for tennantite and bornite in sample W23–115 are –21.92 and –23.91‰, those for enargite and tennantite in sample W23–89b are –15.02 and –16.14‰, respectively, whereas chalcopyrite of sample WW–1a yielded an average $\delta^{34}S$ value of –12.78‰. On the other hand, in cases where the same mineral phase was measured in two different samples (tennantite in W23–89b and in W23–115), S-isotopic variations are much larger (~ 6‰) and far beyond analytical uncertainties. These findings imply that mineral phases were in isotopic equilibrium and that small variations between the individual phases of one sample are either due to analytical uncertainty or to fractionation of the isotope between the minerals. The latter hypothesis has to be tested in a more comprehensive *in situ* isotope study on sulfide minerals in vein-type mineralization from the Wilhelmine mine, as well as from mines at Huckelheim, Grosskahl and Bieber, which is planned for the near future. These tests will be accompanied by extensive conventional analyses of sulfur isotopes in barite and of carbon isotopes in carbonates, from various examples of vein-type mineralization in the Spessart area.

P–T–$a(S_2)$ Conditions of Ore Formation

As the ore veins of the Wilhelmine deposit nearly reach the pre-Permian peneplain, the *lithostatic pressure* that prevailed during the ore-forming process can be roughly estimated from the thickness of the overlying sedimentary strata. These range in age between Upper Permian (Zechstein) to Upper Jurassic (Middle Kimmeridge), when the Spessart area became part of the Rhenish High and was subjected to renewed erosion. Judging from the isopach maps of Freudenberger (1996) and Meyer & Schmidt-Kahler (1996), a maximum total thickness of about 1400 m can be estimated for these sedimentary rocks. If one assumes an average density of 2.5 g/cm^3, this would translate into a lithostatic pressure P_{load} of about 350 bars. If the fault systems hosting the sulfide ore were connected to the surface throughout most of the mineralization, a hydrostatic pressure regime would have prevailed, with $P(H_2O)$ of about 140 bar.

These low pressures should exert only a minimal influence on the equilibrium temperatures of the experi-

mentally determined or theoretically calculated sulfidation-type reactions in the systems Cu – Fe – S and Cu – Fe – As – S (*e.g.*, Cabri 1973, Craig & Barton 1973, Craig & Scott 1974, Barton & Skinner 1979), summarized in the $a(S_2)$ – T diagram (Fig. 11). The absence of pyrrhotite and cubanite (or intermediate solid-solution, *Iss*) and the presence of the assemblage pyrite + chalcopyrite + tennantite in the Wilhelmine ore permits a rough estimate of the *uppermost temperature* that could have been attained during the recrystallization stage. The equilibrium curves of reactions (eq. 1 and 2)

$$\text{pyrite} + \text{chalcopyrite} \rightarrow \textit{Iss} + S_2 \quad (1)$$

and

$$\text{enargite} \rightarrow \text{tennantite} + S_2 \quad (2)$$

cross at about 440°C and $a(S_2) = 10^{-5}$ (Fig. 11). One should recall, however, that the equilibrium curve for reaction (2) is univariant only in the system Cu – As – S. With addition of Sb, Fe and Zn in tennantite, the reaction becomes polyvariant, thus somewhat blurring the cross-over point. Another consequence is that the stable coexistence of enargite + tennantite in some of the samples cannot be used as a buffer assemblage. Nevertheless, it provides a hint of the sulfur activity at a given temperature, *e.g.*, around 10^{-6} at 400°C, ~10^{-8} at 300°C and ~$10^{-11.5}$ at 200°C (Fig. 11). In contrast, pyrite, chalcopyrite and bornite from the Wilhelmine ores have nearly stoichiometric compositions in the system Cu – Fe – S (Table 2, 3, 6). Consequently, their coexistence conforms to the univariant equilibrium (eq. 3)

$$\text{bornite} + \text{pyrite} \rightarrow \text{chalcopyrite} + S_2 \quad (3)$$

buffering the sulfur activity at higher values of $10^{-3.9}$ at 400°C, $10^{-6.7}$ at 300°C and $10^{-10.7}$ at 200°C (Fig. 11). The replacement of bornite and enargite by late tennantite, described above, indicates an increase in temperature or a decrease in the activity of sulfur in the course of the recrystallization stage (Fig. 11).

On the basis of the same mineral assemblages, Schmitt (2001) arrived at a similar maximum tempera-

TABLE 10. RESULTS OF *IN SITU* SULFUR ISOTOPE ANALYSES

Sample	Mineral	Point	$\delta^{34}S$ (‰)	2σ	mean
WW-1a	chalcopyrite	1	-13.21	0.80	
WW-1a	chalcopyrite	2	-12.36	0.80	-12.78
W23-89b	enargite	1	-14.56	0.91	
W23-89b	enargite	2	-15.48	0.91	-15.02
W23-89b	tennantite	1	-15.83	0.91	
W23-89b	tennantite	2	-15.84	0.91	
W23-89b	tennantite	3	-16.75	0.91	-16.14
W23-115	tennantite	1	-22.57	0.97	
W23-115	tennantite	2	-21.27	0.97	-21.92
W23-115	bornite	1	-24.57	0.97	
W23-115	bornite	2	-23.35	0.97	
W23-115	bornite	3	-23.83	0.97	-23.91

The uncertainty is quoted at a level of two standard deviations.

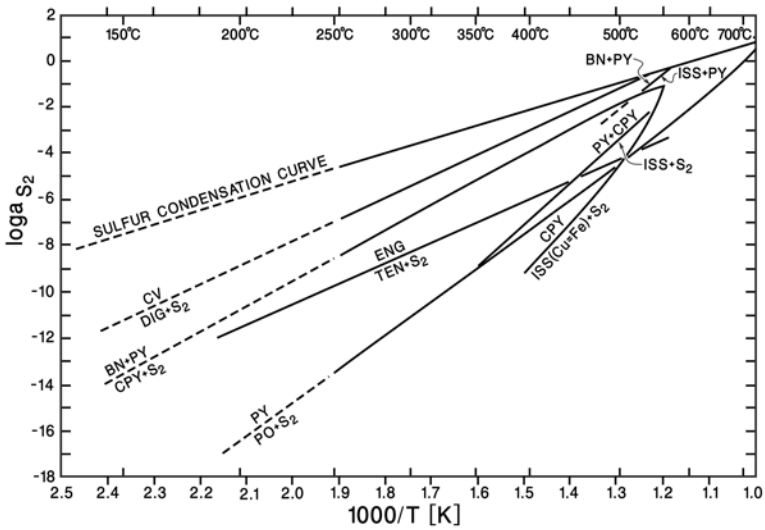

FIG. 11. Log $a(S_2)$–1000/T diagram for phases in the sytems Cu – Fe – S and Cu – Fe – As – S after Barton & Skinner (1979).

ture of about 425°C for the sulfide-vein deposits of Grosskahl and Huckelheim. In contrast, the stable assemblage emplectite + native Bi and the composition of coexisting nickeline and maucherite in the Co–Ni–Bi vein-type mineralization at Bieber, lead to an upper temperature-limit of only ~300°C (Wagner & Lorenz 2002). This agrees much better with temperature estimates for various types of post-Variscan vein deposits in central Europe, based on fluid-inclusion studies, which generally gave formation temperatures below 300°C (*e.g.*, Behr *et al.* 1987, 1993, Lüders & Möller 1992). Unfortunately, an investigation of fluid inclusions in an enargite sample from the Wilhelmine mine, undertaken by Volker Lüders (GFZ Potsdam), was unsuccessful owing to their small size.

The *minimum temperature* attained during the recrystallization stage can be estimated from the very fine-grained or submicroscopic digenite–bornite intergrowths, which indicates that the two phases were unmixed from a homogeneous 1*a* solid solution (Grguric *et al.* 2000). The "spotty" exsolution-texture microscopically observed in the Wilhelmine ore suggests that the initial compositions of the exsolved high digenite were close to the solvus, which is defined, *e.g.*, by Bn_{40} at about 100°C and Bn_{50} at about 150°C (Grguric *et al.* 2000). Electron-microprobe analyses yielded up to 55 mol.% of bornite in these intergrowths. Assuming that the initial composition of the exsolved high digenite was indeed close to the solvus, a composition of Bn_{55} would correspond to about 175°C (Grguric *et al.* 2000; Fig. 10). The shrinkage of the compositional field of $bornite_{ss}$ during cooling led to lamellar (W-type) exsolution of chalcopyrite IIa in large grains of bornite II. Judging from the experiments of Durazzo & Taylor (1982, Fig. 10c), this should have happened at temperatures below about 200°C.

The formation of covellite, yarrowite and spionkopite according to the reversed reaction

$$\text{covellite} \rightarrow \text{digenite} + S_2 \qquad (4)$$

is clearly retrograde and took place under decreasing temperatures or rising activities of sulfur (Fig. 11).

Discussion of the Ore-Forming Process

Geological arguments

From the geological setting of the Wilhelmine mine, either a supergene or a hydrothermal ore-forming process could be considered (Figs. 1b, 2). The close spatial association with the Permian Kupferschiefer, which had overlain the orthogneiss, before erosion, at a vertical distance of only 10–50 m, is an important argument for a genetic link between the Kupferschiefer and the vein-type mineralization in the Wilhelmine mine. Therefore, a supergene ore-forming process, as already claimed by Thürach (1893), seems possible. Such a model would also explain the important observation that the amount of ore decreases from top to bottom, so that ore was no longer recorded in the deeper galleries of the mine (Freymann 1991, Lorenz & Schmitt 2005).

On the other hand, the Spessart area contains numerous veins of barite, which fill SE-trending faults transecting the crystalline basement and the Permo-Triassic sedimentary cover. Like the other vein-type deposits of barite, commonly occurring in central Europe, their hypogene and hydrothermal origin is undisputed (*e.g.*, Murawski 1954, Weinelt 1962, Okrusch & Weinelt 1965, Hess 1973, Hofmann 1979, Lüders *et al.* 1993, Schmitt 1993b) and corroborated by Sr isotope data (see below). Barite veins also occur in the vicinity of the Wilhelmine mine, *i.e.,* between Obersommerkahl and Vormwald and in the upper Speckkahl Valley (Okrusch & Weinelt 1965; see Fig. 2). This close spatial relationship suggests that the barite and the ore veins are the products of the same hydrothermal activity, as already proposed by Bücking (1892). According to radiometric dating of the hydrothermal mineralization at Sailauf, this activity started at about 161 Ma ago, *i.e.,* some 100 Ma *after* the Kupferschiefer sedimentation, and may have lasted, with possible interruptions, until about 98 Ma ago (Hautmann *et al.* 1999). Similar Jurassic and Cretaceous ages have been recorded for various vein-type deposits in central Europe, *e.g.*, in the Harz Mountains (Hagedorn & Lippolt 1993, Haack & Lauterjung 1993) and the Black Forest (Wernicke & Lippolt 1993, 1997).

Textural arguments

The widespread occurrence of colloform textures in the Wilhelmine ore indicates that during the initial stage (I) of the ore-forming process, the sulfide minerals were precipitated from relatively low-temperature solutions which, however, did not necessarily result in colloidal precipitates (Roedder 1968, Harańczyk 1969). Therefore, the colloform textures observed in the Wilhelmine ore cannot be taken as an argument for the assumption of von Gehlen (1964) that the sulfides precipitated from supergene solutions, which seeped into open fissures of the sea floor at the beginning of the Kupferschiefer sedimentation 258 Ma ago. Moreover, the colloform textures of the ore are overgrown and partly obliterated during a later stage of recrystallization (stage II), thus indicating a thermal overprint that can be related to the period of hydrothermal activity in post-Variscan times.

Isotopic constraints

Strontium isotope analyses on four barite samples from veins cross-cutting the Zechstein dolomite at Obersommerkahl yielded $^{87}Sr/^{86}Sr$ values of 0.71141–0.71163, whereas five samples from barite veins in the Lower Buntsandstein of the Spessart gave similar

values, between 0.71146 and 0.7124 (Baumann & Hofmann 1988). These, and comparable results obtained from many barite veins in other parts of central Europe, indicate continental crust as a source, whereas barium transport by supergene solutions derived from seawater can be safely excluded (Baumann & Hofmann 1988).

In situ multicollector LA–ICP–MS analyses of *sulfur isotopes* on individual sulfide minerals in three samples of Wilhelmine ore yielded negative $\delta^{34}S$ values, between –12.8 and –23.9‰, confirming earlier results of Hahn-Weinheimer (in Okrusch & Weinelt 1965). These results indicate a formation by bacterial reduction of sulfate, *e.g.*, during sedimentation and diagenesis of the Kupferschiefer. However, sulfur in the Wilhemine ore is slightly heavier than in the disseminated sulfide minerals from the Kupferschiefer in Germany and southwestern Poland, which display $\delta^{34}S$ values mainly in the range of –25 to –45‰, thus clearly indicating BSR (Marowsky 1969, Harańczyk 1986, Sawlowicz 1989, Bechtel *et al.* 2001). Higher values of $\delta^{34}S$, up to –8.4‰, were recorded from Cu sulfides in high-grade mineralized samples of the German Kupferschiefer and explained by precipitation of metal sulfide through thermochemical reduction of sulfate, accompanied by oxidative degradation of organic matter (Bechtel *et al.* 2001). Sulfides from lenses and veinlets in the Kupferschiefer of southwestern Poland show also consistently higher $\delta^{34}S$ values than the disseminated sulfides (Jowett *et al.* 1991). These authors assumed that hydrothermal sulfur was transported by ore-forming fluids into fault zones and mixed with synsedimentary, ^{34}S-depleted sulfur formed by bacterial reduction of sulfate. Negative $\delta^{34}S$ values, mostly between –8 and –22‰, were also recorded in sulfide minerals of the post-Variscan hydrothermal Pb–Zn deposit of St. Andreasberg, Harz Mountains, and explained by an uptake of biogenic sulfur from sedimentary country-rocks through ore-forming fluids (Zheng & Hoefs 1993). By analogy, we propose that the sulfides in the Wilhelmine mine were leached from the Kupferschiefer by hydrothermal fluids, whereby either thermochemical reduction of sulfate or an admixture of some hydrothermal sulfur caused a slight increase in the $\delta^{34}S$ values compared to those of the Kupferschiefer sulfides.

Source of metals

Recent models for the genetic interpretation of post-Variscan barite – fluorite – sulfide veins in central Europe, based on fluid-inclusion and stable isotope studies, assume two different reservoirs of ore-forming solutions (*e.g.*, Behr *et al.* 1987, Lüders *et al.* 1993, Zheng & Hoefs 1993): (i) metal-bearing, highly saline brines of deep origin in the basement, acting as solvents for metals, barium and fluorine, were repeatedly mixed at different ratios with (ii) cooler, low-salinity formation waters carrying H_2S, during the sulfide stage, and SO_4^{2-}, during the later crystallization of barite. The formation waters were probably derived from Permo-Triassic sedimentary sequences containing abundant intercalations of anhydrite. As there is little doubt that barite formed as a result of this mixing process, the question remains whether the metal content of the ore veins has been transported with the basement brines from a deeper reservoir or was derived by leaching of the overlying Kupferschiefer. In both models, one assumes that the hydrothermal brines, having penetrated the crystalline basement along NW–SE fracture zones, reached the level of the Kupferschiefer and dolomites of the Werra cycle, whereas the clays and marls of the Leine and Aller cycle in places acted as a barrier, not penetrated by the brine. Consequently, these brines had ample time to infiltrate the Kupferschiefer, along faults and cracks, allowing them to react with its organic and mineral constituents.

A *modified hydrothermal model* is based on the fact that the Kupferschiefer is markedly enriched in iron and base metals compared to other bituminous clays and claystones (*e.g.*, Wedepohl 1964, Kucha 1990). Therefore, Fe, Cu, As, Sb, Bi, Zn, Hg and Ag could have been leached, together with sulfur, out of the Kupferschiefer by hydrothermal basement brines. However, such a model does not explain the distinct differences in metal content and ore mineralogy recorded for the various examples of Kupferschiefer-related vein-type mineralization of the Spessart, *i.e.,* Cu–Fe–As at Wilhelmine mine, Cu–As–Ag–Pb–Zn at Huckelheim–Grosskahl, Ba–Co–Ni at Huckelheim, Co–Ni–Bi at Bieber and Mn–As–Bi at Sailauf. These differences suggest individual, deep-seated reservoirs for the ore-forming fluids rather than a uniform reservoir of the Kupferschiefer.

We, therefore, prefer a *strictly hydrothermal model* according to which the metal content is derived from deeper sources and transported by the ore-forming fluids. A well-investigated example is the hydrothermal transport of *arsenic*, which plays an important role not only in the Wilhelmine deposit, with tennantite and enargite as important ore minerals, but also for the deposits at Grosskahl, Huckelheim and Bieber (Schmitt 2001, Wagner & Lorenz 2002). Considerable concentrations of the As^{3+} species have been recorded in fluids of active geothermal systems (*e.g.*, Ballantyne & Moore 1988, Wood & Samson 1998), including the deep-seated thermal system at the southern margin of the Rhenish Massif, Germany (Schwenzer *et al.* 2001, Wagner *et al.* 2005). This spring system may be regarded as a modern analogue to the basement-derived mineralizing fluids produced during the hydrothermal activity in Middle Jurassic to late Early Cretaceous times. Experimental investigations have shown that, in ore-forming fluids, arsenic is transported as oxidized As^{3+} species such as $H_3AsO_3^0$, $H_2AsO_3^-$, $H_2AsO_3^{2-}$ and AsO_3^{3-}, and that reduction of these fluids causes precipitation of As sulfides (*e.g.*, Ballantyne & Moore 1988, Pokrovski *et al.* 1996). A similar process can be envisaged for the precipitation of Cu, which presumably is transported

in the form of chloride complexes like $CuCl_2^-$ (Wood & Samson 1998). On the basis of analytical results on the hydrocarbons, Jochum (2000) developed a model according to which sulfide minerals in post-Variscan veins of the Rhenish Massif were precipitated by thermochemical reduction of sulfate, caused by interaction of the hydrothermal fluids with organic matter in the country rocks. In addition, precipitation could have been achieved by an increase in pH due to reaction of hydrothermal solutions with the carbonate content of the Kupferschiefer (*e.g.*, Seward & Barnes 1997).

In the case of the Wilhelmine ore, the deep-sourced metal-bearing basement brines infiltrated the orthogneiss under oxidizing conditions, as indicated by the alteration assemblage hematite – white mica. After having reached the overlying Kupferschiefer, the hydrothermal fluids reacted with sulfur-bearing organic matter, pyrite and carbonates, leading to the thermochemical reduction of sulfate and increase of pH, and, consequently, precipitation of sulfide minerals (Lorenz & Schmitt 2005). A similar model was recently invoked by Wagner & Lorenz (2002) to explain the close spatial association of the Co–Ni–Bi vein mineralization at Bieber with the Permian Kupferschiefer. Interestingly, a similar model has been recently proposed to explain the unusual enrichment of Cu in the Kupferschiefer shales of the Lubin district, southwestern Polish basin. According to Blundell *et al.* (2003), this metal concentration is related to a localized high heat-flow anomaly. Triggered by co-seismic strain and normal faulting, pulses of hot, Cu-bearing brines derived from a deep-seated fault-fracture system were injected into the porous lower Permian (Rotliegend) sandstones and the immediately overlying Kupferschiefer shale, where chemical conditions allowed precipitation of the metals from the brine.

Summary and Conclusions

1. Cu-rich sulfide ore veins in the former Wilhelmine mine at Sommerkahl, with pyrite, tennantite, enargite, chalcopyrite, bornite and digenite as important ore minerals, are hosted by orthogneisses of the Spessart Crystalline Complex and are overlain by Permo-Triassic sedimentary strata including, the Upper Permian Kupferschiefer. This close spatial association suggests a genetic link between the Kupferschiefer and the vein-type mineralization. On the other hand, the ore veins are closely associated with barite veins of undisputed hydrothermal origin.

2. Colloform textures in the Wilhelmine ore testify to an early stage (I) of the ore-forming process, with precipitation from low temperature, but not necessarily supergene solutions. Recrystallization took place at a later stage (II), in which the colloform textures were partly obliterated. Stage II relates to a period of thermal overprint, presumably with rising temperatures.

3. On cooling, the compositional field of initial high-temperature bornite (1*a* solid solution) was reduced, leading to fine-grained ("spotty") to submicroscopic bornite–digenite intergrowths. From their maximum bornite content of about 55 mol.%, a minimum temperature of about 175°C can be estimated for the recrystallization stage. The upper stability-limit of the assemblage tennantite + chalcopyrite + pyrite leads to a temperature maximum of 440°C which, however, was presumably never reached during the ore-forming process.

4. *In situ* sulfur isotope analyses of various sulfide phases in the Wilhelmine ore yielded negative $\delta^{34}S$ values, between –23.9 and –12.8‰. These values indicate that sulfur of the Wilhelmine sulfides was derived from the overlying Kupferschiefer, but was isotopically modified by thermochemical sulfate reduction (TSR) or mixing with some hydrothermal sulfur.

5. By analogy, one could argue that the metal content of the Wilhelmine ore was leached out of the Kupferschiefer. However, compositional differences among the various examples of Kupferschiefer-related vein-type mineralization in the Spessart make such a common reservoir unlikely. We therefore prefer an alternative model, according to which the metals were transported from deep-seated reservoirs by basement brines. We assume that precipitation of the metal sulfides were caused by thermochemical sulfate reduction (TSR), due to interaction of the hydrothermal fluids with the overlying Kupferschiefer.

6. Like in other parts of the Variscan Orogen, the Cu-rich sulfide ore veins of the Wilhelmine mine are the result of post-Variscan hydrothermal activity that affected the Spessart area in Middle Jurassic to late Early Cretaceous times, between *ca.*161 and 98 Ma.

Acknowledgements

We are greatly indepted to Hans Joachim Lippolt for allowing us to use unpublished (U/Th)–He and K–Ar data produced in his laboratory. We thank Yann Lahaye and Chris Bendall for discussions and advice on sulfur isotope measurements, Uli Schüssler for advice and help with the electron microprobe, and Rainer Hock, Klaudia Hradil and Armin Zeh for their help with X-ray diffraction. The painstaking efforts of Volker Lüders to analyze the fluid inclusions in an enargite sample of the Wilhelmine mine are gratefully acknowledged. Thanks are due to Martin Hanauer, Werner Schaupert and Thomas Weis for providing important samples, to Klaus-Peter Kelber for the photographs and part of the line drawings, and to Peter Späthe for careful preparation of the polished sections. The first draft of this paper was critically read by Hartwig Frimmel, Ulrich Hein, Ralf T. Schmitt and Thomas Wagner; their suggestions improved the paper considerably and are highly appreciated. We are also indepted to Andrew Conly, David Lentz and an anonymous reviewer for their constructive

and helpful reviews and to Robert F. Martin for careful editorial handling.

References

Ballantyne, J.M. & Moore, J.N. (1988): Arsenic geochemistry in geothermal systems. *Geochim. Cosmochim. Acta* **52**, 475-483.

Barton, P.B., Jr. (1973): Solid solutions in the system Cu–Fe–S. I. The Cu–S and CuFe–S join. *Econ. Geol.* **68**, 455-465.

Barton, P.B., Jr. & Skinner, B.J. (1979): Sulfide mineral stabilities. *In* Geochemistry of Hydrothermal Ore Deposits (2nd ed., H.L. Barnes, editor). J. Wiley & Sons, New York, N.Y. (278-403).

Baumann, A. & Hofmann, R. (1988): Strontium isotope systematics of hydrothermal vein minerals in deposits of West Germany. *Geol. Rundschau* **77**, 747-762.

Bechtel, A., Sun, Yuszhuang, Püttmann, W., Hoernes, S. & Hoefs, J. (2001): Isotopic evidence for multi-stage metal enrichment in the Kupferschiefer from the Sangershausen Basin, Germany. *Chem. Geol.* **176**, 31-49.

Behr, H.J., Gerler, J., Hein, U.F. & Reutel, C.J. (1993): Tectonic brines and basement brines in den mitteleuropäischen Variszide: Herkunft, metallogenetische Beutung und geologische Aktivität. *Göttinger Arb. Geol. Paläont.* **58**, 3-28.

Behr, H.J., Horn, E.E., Frentzel-Beyme, K. & Reutel, C.J. (1987): Fluid inclusion characteristics of the Variscan and post-Variscan mineralizing fluids in the Federal Republic of Germany. *Chem. Geol.* **61**, 273-285.

Bendall, C., Lahaye, Y., Fiebig, J., Weyer, S. & Brey, G.P. (2006): In-situ sulfur isotope analysis by laser-ablation MC–ICPMS. *Appl. Geochem.* **21**, 782-787.

Bundell, D.J., Karnkowski, P.H., Alderton, D.H.M., Oszczepalkski, S. & Kucha, H. (2003): Copper mineralization of the Polish Kupferschiefer: a proposed basement fault – fracture system of fluid flow. *Econ. Geol.* **98**, 1487-1495.

Bücking, H. (1892): Der nordwestliche Spessart. *Jahrb. preuß. geol. Landesanst. N.F.* **12**, 1-274 .

Cabri, L.J. (1973): New data on phase relations in the Cu – Fe – S system. *Econ. Geol.* **68**, 443-454.

Craig, J.R. & Barton, P.B., Jr. (1973): Thermochemical approximations of sulfosalts. *Econ. Geol.* **68**, 493-506.

Craig, J.R. & Scott, S.D. (1974): Sulfide phase equilibria. *In* Sulfide Mineralogy (P.H. Ribbe, ed.). *Mineral. Soc. Am., Short Course Notes* **1**, CS-1 – CS-110.

Diederich, H. & Laemmlen, M. (1964): Das obere Biebertal im Nordspessart. Neugliederung des Unteren Buntsandsteins, Exkursionsführer und geologische Karte. Mit einem Beitrag von Villwock, R. *Abhandl. hess. Landes-Amt Bodenforsch.* **48**, 1-34.

Dill, H. (1988): Geologic setting and age relationship of fluorite–barite mineralization in southern Germany with special reference to the Late Paleozoic unconformity. *Mineral. Deposita* **23**, 16-23.

Dombrowski, A., Henjes-Kunst, F., Höhndorf, A., Kröner, A., Okrusch, M. & Richter, P. (1995): Orthogneisses in the Spessart Crystalline Complex, northwest Bavaria: Silurian granitoid magmatism at an active continental margin. *Geol. Rundschau* **84**, 399-411.

Dombrowski, A., Okrusch, M. & Henjes-Kunst, F. (1994): Geothermometry and geochronology on mineral assemblages in orthogneisses and related metapelites of the Spessart Crystalline Complex, NW Bavaria, Germany. *Chem. Erde* **54**, 85-101.

Durazzo, A. & Taylor, L.A. (1982): Experimental exsolution textures in the system bornite–chalcopyrite: genetic implications concerning natural ores. *Mineral. Deposita* **17**, 79-97.

Evans, H.T., Jr. (1979): The crystal structures of low chalcocite and djurleite. *Z. Kristallogr.* **150**, 299-320.

Frenzel, G. (1959): Idait und "blaubleibender Covellin". *Neues Jahrb. Mineral., Abh.* **93**, 87-132.

Freudenberger, W. (1996): Gesteinsfolge des Deckgebirges nördlich der Donau und im Molasseuntergrund. Perm, Trias. *In* Erläuterungen zur Geologische Karte von Bayern 1:500 000 (W. Freudenberger & K. Schwerd, eds.). Bayerisches Geologisches Landesamt, München, Germany. (55-89).

Freymann, K. (1991): Der Metallerzbergbau im Spessart. *Veröffentl. Geschichts- und Kunstverein Aschaffenburg* **33**, 1-413.

Fritz, J. (1895) Mineralogische Aufzeichnungen aus dem Gebiete des Vorspessarts. *Berichte Wetterauische Gesellschaft gesamte Naturkunde* **1892-1895**, 77-81.

Gerlach, R. (1992): Kluftgebundene Mineralisationen im subsalinaren Tafeldeckgebirge des Harzvorlandes – Lagerstättentyp Mansfelder Rücken. *Z. geol. Wiss.* **20**, 233-238.

German Stratigraphic Commission (2002): Stratigraphic Table of Germany 2002. GeoForschungsZentrum, Potsdam, Germany.

Goble, R.J. (1980): Copper sulfides from Alberta: yarrowite, Cu_9S_8, and spionkopite $Cu_{39}S_{28}$. *Can. Mineral.* **18**, 511-518.

Goble, R.J. (1981): The leaching of copper from anilite and the production of a metastable copper sulfide structure. *Can. Mineral.* **19**, 583-592.

Goble, R.J. & Robinson, G. (1980) Geerite $Cu_{1.60}S$, a new copper sulfide from Dekalb Township, New York. *Can. Mineral.* **18**, 519-523.

Goble, R.J. & Smith, D.G.W. (1973): Electron microprobe investigation of copper sulfides in the Precambrian Lewis Series of S.W. Alberta, Canada. *Can. Mineral.* **12**, 95-103.

Grguric, B.A., Harrison, R.J. & Putnis, A. (2000): A revised phase diagram for the bornite–digenite join from *in situ* neutron diffraction and DSC experiments. *Mineral. Mag.* **64**, 213-231.

Haack, U. & Lauterjung, J. (1993): Rb/Sr dating of hydrothermal overprint in Bad Grund by mixing lines. *In* Formation of Hydrothermal Vein Deposits. A case study of the Pb–Zn, barite and fluorite deposits of the Harz Mountains (P. Möller & V. Lüders, eds.). *In* Monograph Series on Mineral Deposits **30**, Borntraeger, Berlin, Germany (103-112).

Hagedorn, B. & Lippolt, H.J. (1993): Isotopic age constraints for epigenetic mineralizations in the Harz Mountains (Germany) from K–Ar, $^{40}Ar/^{39}Ar$ and Rb–Sr data of authigenic K-feldspars. *In* Formation of Hydrothermal Vein Deposits. A case study of the Pb–Zn, barite and fluorite deposits of the Harz Mountains (P. Möller & V. Lüders, eds.). *In* Monograph Series on Mineral Deposits **30**, Borntraeger, Berlin, Germany (87-102).

Harańczyk, C. (1969): Noncolloidal origin of colloform textures. Discussion on the paper Roedder (1968). *Econ. Geol.* **64**, 466-468.

Harańczyk, C. (1986): Zechstein copper-bearing shales in Poland. Lagoonal environments and the sapropel model of genesis. *In* Geology and Metallogeny of Copper Deposits (G.H. Friedrich *et al.*, eds). *S.G.A. Spec. Publ.* **4**, 461-476.

Hartmann, R. & Harris, M.F. (1985): Exploration for metamorphosed sediment-hosted massive sulfide deposits in the crystalline Spessart. *Fortschr. Mineral.* **63**, *Beiheft* 1, 85.

Hautmann, S., Brander, H., Lippolt, H.J. & Lorenz, J (1999): K–Ar and (U+Th)–He chronometry of multistage alteration and mineralisation in the Hartkoppe rhyolite, Spessart, Germany. *J. Conf. Abstr.* **4**, 769.

Hess, G. (1973): Zum geologisch-tektonischen Rahmen der Schwerspatlagerstätten im Südharz und Spessart. *Geol. Jahrb.* **D4**, 3-65.

Hofmann, R. (1979): Die Entwicklung der Abscheidungen in den gangförmigen, hydrothermalen Barytvorkommen Mitteleuropas. *In* Zur Minerogenie des hydrothermalen Baryts in Deutschland. *In* Monograph Series on Mineral Deposits **17**, Borntraeger, Berlin, Germany (81-214).

Jochum, J. (2000): Variscan and post-Variscan lead–zinc mineralization, Rhenish Massif, Germany: evidence for sulfide precipitation via thermochemical sulfate reduction. *Mineral. Deposita* **35**, 451-454.

Jowett, R.C., Rye, R.O., Rydzewski, A. & Oszczepalski, S. (1991): Isotopic evidence for the addition of sulfur during formation of the Kupferschiefer ore deposits in Polen. *Zentralbl. Geol. Paläont.* Teil I, **1991**, 1001-1015.

Koto, K. & Morimoto, M. (1970): The crystal structure of anilite. *Acta Crystallogr.* **B26**, 915-924.

Koto, K. & Morimoto, M. (1975): Superstructure investigation of bornite, Cu_5FeS_4, by the modified partial Patterson function. *Acta Crystallogr.* **B31**, 2268-2273.

Kreuzer, H., Lenz, H., Harre, W., Matthes, S., Okrusch, M. & Richter, P. (1973): Zur Altersstellung der Rotgneise im Spessart, Rb/Sr-Gesamtgesteinsdatierungen. *Geol. Jahrb.* **A9**, 69-88.

Kucha, H. (1990): Geochemistry of the Kupferschiefer, Poland. *Geol. Rundschau* **79**, 387-399.

Kulick, J., Leifeld, D., Meisl, S., Pöschl, W., Stellmacher, R., Strecker, G., Theuerjahr, A.-K. & Wolf, M. (1984): Petrofazielle und chemische Erkundung des Kupferschiefers der Hessischen Senke und des Harz-Westrandes. *Geol. Jahrb.* **D68**, 3-223.

Lippolt, H.J. (1986): Nachweis altpaläozoischer Primäralter (Rb–Sr) und karbonischer Abkühlungsalter (K–Ar) der Muskovit–Biotit-Gneise des Spessarts und der Biotit-Gneise des Böllsteiner Odenwaldes. *Geol. Rundschau* **75**, 569-583.

Lorenz, J. (1991): Die Mineralien im Rhyolith von Sailauf – eine Ergänzung. *Aufschluss* **42**, 1-38.

Lorenz, J. (1995): Mineralisationen aus dem Rhyolith-Steinbruch von Sailauf einschließlich der Neufunde von ged. Arsen, Bertrandit, Humboldtin und Tilasit. *Aufschluss* **46**, 105-122.

Lorenz, J. (2004): Sailaufit, Rhodochrosit, Kaatialait, Bixbyit, Takanelit, ged. Wismut und weitere Neufunde aus dem Rhyolith-Steinbruch in der Hartkoppe bei Sailauf im Spessart. *Mineralien-Welt* **15**(4), 21-33, **15**(5), 26-38.

Lorenz, J. & Schmitt, R.T. (2005): Das Kupfererzbergwerk der Grube "Wilhelmine" in Sommerkahl. Mineralien aus der Grube Wilhelmine. *Spessart* **99** (Febr.), 3-22, 25-32.

Lüders, V., Gerler, J., Hein, U.F. & Reutel, C.J. (1993): Chemical and thermal development of ore-forming solutions in the Harz Mountains: a summary of fluid inclusion studies. *In* Formation of hydrothermal vein deposits – a case study of the Pb–Zn, barite and fluorite deposits of the Harz Mountains (P. Möller & V. Lüders, eds.). *In* Monograph Series on Mineral Deposits **30**. Borntraeger, Berlin, Germany (117-132).

Lüders, V. & Möller, P. (1992): Fluid evolution and ore deposition in the Harz Mountains (Germany). *Eur. J. Mineral.* **4**, 1053-1068.

Marowsky, G. (1969): Schwefel-, Kohlenstoff- und Sauerstoff-Isotopenuntersuchungen am Kupferschiefer als

Beitrag zur genetischen Deutung. *Contrib. Mineral. Petrol.* **22**, 290-334.

MASKE, S. & SKINNER, B.J. (1971): Studies of the sulfosalts of copper. I. Phases and phase relations in the system Cu – As – S. *Econ. Geol.* **66**, 901-918.

MATTHES, S. & OKRUSCH, M. (1965): Petrographische Untersuchung zur Frage der Rotgneise im Spessart. *Geologie* **14**, 1148-1200.

MESSER, E. (1955): Kupferschiefer, Sanderz und Kobaltrücken im Richelsdorfer Gebirge (Hessen). *Hess. Lagerstättenarchiv* **3**, 1-127.

MEYER, R.K.F. & SCHMIDT-KAHLER, H. (1996): Gesteinsfolge des Deckgebirges nördlich der Donau und im Molasseuntergrund. Jura. *In* Erläuterungen zur Geologische Karte von Bayern 1:500 000 (W. Freudenberger & K. Schwerd, eds.). Bayerisches Geologisches Landesamt, München, Germany (90-111).

MORIMOTO, N. (1962): Djurleite, a new copper sulfide mineral. *Mineral. J.* **3**, 338-344.

MORIMOTO, N. & GYOBU, A. (1971): The composition and stability of digenite. *Am. Mineral.* **56**, 1889-1909.

MORIMOTO, N. & KOTO, K. (1970): Phase relations of the Cu–S system at low temperatures: stability of anilite. *Am. Mineral.* **55**, 106-117.

MORIMOTO, N., KOTO, K. & SHIMAZAKI, Y. (1969): Anilite, Cu_7S_4, a new mineral. *Am. Mineral.* **54**, 1256-1268.

MORIMOTO, N. & KULLERUD, G. (1966): Polymorphism on the Cu_9S_5–Cu_5FeS_4 join. *Z. Kristallogr.* **123**, 235-254.

MURAWSKI, H. (1954): Bau und Genese von Schwerspatlagerstätten des Spessart. *Neues Jahrb. Geol. Paläont., Monatsh.*, 145-163.

NASIR, S., OKRUSCH, M., KREUZER, H., LENZ, H. & HÖHNDORF, A. (1991): Geochronology of the Spessart crystalline complex, Mid-German crystalline rise. *Mineral. Petrol.* **43**, 39-55.

OKRUSCH, M. (1995): IV Mid-German Crystalline High. IV.E. Metamorphic evolution. *In* Pre-Permian Geology of Central and Eastern Europe (R.D. Dallmeyer, W. Franke & K. Weber, eds.). Springer, Berlin, Germany (201-213).

OKRUSCH, M. & RICHTER, P. (1986): Orthogneisses of the Spessart crystalline complex, northwest Bavaria: indicators of the geotectonic environment. *Geol. Rundschau* **75**, 555-568.

OKRUSCH, M., STREIT, R. & WEINELT, W. (1967): Erläuterungen zur Geologischen Karte von Bayern 1:25000, Blatt 5920 Alzenau. Bayerisches Geologisches Landesamt, München, Germany (1-336).

OKRUSCH, M. & WEBER, K. (1996): Der Kristallinkomplex des Vorspessart. *Z. geol. Wiss.* **24**, 141-174.

OKRUSCH, M. & WEINELT, W. (1965): Erläuterungen zur Geologischen Karte von Bayern 1:25000, Blatt 5921 Schöllkrippen. Bayerisches Geologisches Landesamt, München, Germany (1-327).

PAUL, J. (1982): Zur Rand- und Schwellenfazies des Kupferschiefers. *Z. deutsche geol. Ges.* **133**, 571-605.

PAUL, J. (1985): Stratigraphie und Fazies des südwestdeutschen Zechsteins. *Geol. Jahrb. Hessen* **113**, 59-73.

POKROVSKI, G., GOUT, R., SCHOTT, J., ZOTOV, A. & HARRICHOURI, J.C. (1996): Thermodynamic properties and stoichiometry of As(III) hydroxide complexes at hydrothermal conditions. *Geochim. Cosmochim. Acta* **60**, 737-749.

POTTER, R.W., II (1977): An electrochemical investigation of the sytem copper–sulfur. *Econ. Geol.* **72**, 1524-1542.

PRÜFERT, J. (1969): Der Zechstein im Gebiet des Vorspessarts und der Wetterau. *Sonderveröffentl. Geolog. Inst. Univ. Köln* **16**, 1-176.

ROEDDER, E. (1968): The noncolloidal origin of "colloform" textures in sphalerite ores. *Econ. Geol.* **63**, 451-471.

ROSEBOOM, E.H., JR. (1962): Djurleite, $Cu_{1.96}S$, a new mineral. *Am. Mineral.* **47**, 1181-1184.

ROSEBOOM, E.H., JR. (1966): An investigation in the system Cu–S and some natural copper sulfides between 25° and 700°C. *Econ. Geol.* **61**, 641-672.

SAWLOWICZ, Z. (1989): On the origin of copper mineralization in the Kupferschiefer: a sulfur isotope study. *Terra Nova* **1**, 339-343.

SCHMIDT, F.P. & FRIEDRICH, G.H. (1988): Geologic setting and genesis of Kupferschiefer mineralization in West Germany. *In* Base Metal Sulfide Deposits in Volcanic and Sedimentary Environments (G.H. Friedrich & P.M. Herzig, eds.). *S.G.A., Spec. Publ.* **6**, 25-59.

SCHMIDT, F.P., SCHUMACHER, C., SPIETH, V. & FRIEDRICH, G. (1986): Results of recent exploration for copper–silver deposits in the Kupferschiefer of West Germany. *In* Geology and Metallogeny of Copper Deposits (G.H. Friedrich *et al.*, eds.). *S.G.A. Spec. Publ.* **4**, 572-582.

SCHMITT, R.T. (1991): Buntmetallmineralisation im Zechstein 1 (Werra-Folge) des nordwestlichen Vorspessarts (Großkahl – Huckelheim – Altenmittlau). *Diploma thesis Univ Würzburg, Germany.*

SCHMITT, R.T. (1992): Die Grube Hilfe Gottes bei Großkahl im Spessart. *Aufschluss* **43**, 309-318.

SCHMITT, R.T. (1993a): Sulfide und Arsenide aus den Gruben Segen Gottes bei Huckelheim und Hilfe Gottes bei Großkahl im Spessart. *Aufschluss* **44**, 111-122.

SCHMITT, R.T. (1993b): Wismutminerale aus den Barytgängen des Spessarts. *Aufschluss* **44**, 329-336.

SCHMITT, R.T. (2001): Zur Petrographie, Geochemie und Buntmetallmineralisation des Zechstein-1 (Werra–Folge) im Gebiet Huckelheim – Großkahl (Nordwestlicher Spessart). *Mitteilungen Naturwiss. Museum Stadt Aschaffenburg* **20**, 1-100.

SCHUMACHER, C., KAIDIES, E. & SCHMIDT, F.-P. (1984): Der basale Zechstein der Spessart–Rhön-Schwelle. *Z. deutsche geol. Ges.* **135**, 563-571.

SCHWENZER, S.P., TOMMASEO, C.E., KERSTEN, M. & KIRNBAUER, T. (2001): Speciation and oxidation kinetics of arsenic in thermal springs of Wiesbaden spa, Germany. *Fresenius J. Anal. Chem.* **371**, 927-933.

SEWARD, T.M. & BARNES, H.L. (1997): Metal transport by hydrothermal ore fluids. *In* Geochemistry of Hydrothermal Ore Deposits (3rd ed., H.L. Barnes, editor). John Wiley & Sons, New York, N.Y. (435-486).

SHEPHERD, T.J., BOUCH, J.E., GUNN, A.G., MCKERVEY, J.A., NADEN, J., SCRIVENER, R.C., STYLES, M.T. & LARGE, D.E. (2005) : Permo-Triassic unconformity-related Au–Pd mineralisation, South Devon, UK: new insights and the European perspective. *Mineral. Deposita* **40**, 24-44.

SPECZIK, S. (1995): The Kupferschiefer mineralization of central Europe: new aspects and major areas of future research. *Ore Geol. Rev.* **9**, 411-426.

TOBSCHALL, H.J., SCHMIDT, F.P. & SCHUMACHER, C. (1986): Exkursion C2; Kupferschiefer und Kupfervererzungen im Richelsdorfer Gebirge, Hessen. Ihre Entstehung im Rahmen der sedimentären Entwicklung des basalen Zechsteins. *Fortschr. Mineral.* **64**(2), 143-160.

THÜRACH, H. (1893): Über die Gliederung des Urgebirges im Spessart. *Geognostische Jahreshefte* **5**, 1-160.

UDLUFT, H. (1923): Zur Entstehung der Eisen- und Manganerze des oberen Zechsteins in Spessart und Odenwald. *Senckenbergiana* **5**, 184-207.

VAUGHAN, D.J., SWEENY, M., FRIEDRICH, G., DIEDEL, R. & HANCZYK, C. (1989): The Kupferschiefer: an overview with an appraisal of the different types of mineralization. *Econ. Geol.* **84**, 1003-1027.

VON GEHLEN, K. (1964): Anomaler Bornit und seine Umbildung zu Idait und "Chalkopyrit" in deszendenten Kupfererzen von Sommerkahl (Spessart). *Fortschr. Mineral.* **41**, 163.

WAGNER, T., KIRNBAUER, T., BOYCE, A.J. & FALLICK, A.E. (2005): Barite–pyrite mineralization of the Wiesbaden thermal spring system, Germany: a 500-kyr record of geochemical evolution. *Geofluids* **5**, 124-139.

WAGNER, T. & LORENZ, J. (2002): Mineralogy of complex Co–Ni–Bi vein mineralization, Bieber deposit, Spessart, Germany. *Mineral. Mag.* **66**, 385-407.

WEDEPOHL, K.H. (1964): Untersuchungen am Kupferschiefer in Nordwestdeutschland: ein Beitrag zur Deutung der Genese bituminöser Sedimente. *Geochim. Cosmochim. Acta* **28**, 305-364.

WEIDMANN, C. (1929): Zur Geologie des Vorspessarts. Lithogenetische und tektonische Untersuchungen. *Rhein-Mainische Forschungen* **3**, 1-74.

WEINELT, W. (1962): Erläuterungen zur Geologischen Karte von Bayern 1:25000, Blatt 6021 Haibach. Bayerisches Geologisches Landesamt, München, Germany (1-246).

WERNICKE, R. S. & LIPPOLT, H.J. (1993): Botryoidal hematite from the Schwarzwald (Germany): heterogeneous uranium distributions and their bearing on the helium dating method. *Earth Planet. Sci. Lett.* **114**, 287-300.

WERNICKE, R. S. & LIPPOLT, H.J. (1997): (U+Th) – He evidence of Jurassic continuous hydrothermal activity in the Schwarzwald basement, Germany. *Chem. Geol.* **138**, 273-285.

WEYER, S. & SCHWIETERS, J. (2003): High precision Fe isotope measurements with high mass resolution MC–ICPMS. *Int. J. Mass Spectrom.* **226**, 355-368.

WILL, T.M. (1998): Phase diagrams and their application to determine pressure–temperature paths of metamorphic rocks. *Neues Jahrb. Mineral., Abh.* **174**, 103-130.

WOOD, S.A. & SAMSON, I.M. (1998): Solubility of ore minerals and complexation of ore metals in hydrothermal solutions. *Rev. Econ. Geol.* **10**, 33-76.

ZHENG, Y.F. & HOEFS, J. (1993): Stable isotope geochemistry of hydrothermal mineralizations in the Harz Mountains. II. Sulfur and oxygen isotopes of sulfides and sulfate and constraints on metallogenetic models. Formation of hydrothermal vein deposits – a case study of the Pb–Zn, barite and fluorite deposits of the Harz Mountains. *In* Monograph Series on Mineral Deposits **30** (P. Möller & V. Lüders, eds.). Borntraeger, Berlin, Germany (211-229).

ZIEGLER, P.A. (1987): Geodynamic model for Alpine intraplate compressional deformation in western and central Europe. *Geol. Soc., Spec. Publ.* **44**, 63-85.

Received October 21, 2005, revised manuscript accepted December 24, 2006.